International Journal of Heat and Mass Transfer 263 (2026) 128625

Contents lists available at ScienceDirect

International Journal of Heat and Mass Transfer

journal homepage: www.elsevier.com/locate/ijhmt

Parametric effects of surface roughness, material, size, orientation, pressure, and subcooling on different regimes of cryogenic pool boiling curve in terrestrial gravity

Faraz Ahmad [a], Issam Mudawar [*,a], Michael Meyer [b], Jason Hartwig [c]

[a] Purdue University Boiling and Two-Phase Flow Laboratory (PU-BTPFL), School of Mechanical Engineering, Purdue University, 585 Purdue Mall, West Lafayette, IN 47907, USA
[b] MTS Inc., 3495 Kent Ave, West Lafayette, IN 47906, USA
[c] Fluids and Cryogenics Branch, NASA Glenn Research Center, Cleveland, OH 44135, USA

ARTICLE INFO

Keywords:
Parametric study
Surface size
Surface material
Surface orientation
Surface roughness
Subcooling
Terrestrial gravity
Cryogenic pool boiling

ABSTRACT

This study builds upon the authors' prior work on cryogenic pool boiling, which established baseline heat transfer coefficient (HTC) correlations for nucleate boiling (NB), transition boiling (TB), and film boiling (FB), as well as correlations for the critical heat flux (CHF) and minimum heat flux (MHF). While the earlier work focused exclusively on baseline conditions, the present study extends those findings by incorporating the parametric effects of subcooling and key system characteristics, namely pressure, surface roughness, material, size, and orientation of the heated surface. Updated correlations for the boiling regimes and transition points were developed based on an expanded database compiled from the literature. The data revealed that the minimum dimension of the heated surface (L_c) has a significant influence on the FB HTC, as well as CHF and MHF when L_c is less than three times Taylor's most dangerous wavelength (λ_d), but approach asymptotic values beyond this threshold. For example, applying the effect of heated surface length in FB HTC reduces the MAE for LH_2 from 33.71% to 12.77%. Moreover, surface roughness is found to strongly affect the NB regime, while exerting negligible impact on the other regimes. Specifically, the inclusion of a surface roughness multiplier in the NB correlation reduces MAE from 47.68% to 22.43% for rough surface data. Increasing the thermal conductivity of the heating surface enhances both the CHF and NB HTC but reduces the MHF. Due to the absence of direct contact between the liquid and the surface, the FB regime is largely unaffected by surface properties. Subcooling is shown to enhance heat transfer across all boiling regimes. To capture all these effects, multiplier functions were introduced to modify the previous baseline correlations for each boiling regime and transition points. The updated correlations demonstrate excellent agreement with experimental data and extend the applicability of the authors' previous models to realistic cryogenic boiling scenarios involving diverse configurations.

1. Introduction

1.1. Background

The continuous advancement of modern technologies has posed significant challenges for thermal engineers, driven by the growing demand for compact, high-performance cooling solutions. As electronic systems, power devices, and cryogenic technologies continue to evolve toward higher power densities and lower operating temperatures, effective thermal management has become a critical bottleneck for ensuring system reliability and efficiency. Over the years, researchers have developed innovative cooling strategies and explored diverse heat transfer enhancement mechanisms to meet these escalating demands. A major contributor to this global effort is Purdue University's Boiling and Two-Phase Flow Laboratory (PU-BTPFL), which has devoted more than four decades to advancing the science and engineering of boiling heat transfer. PU-BTPFL's research encompasses virtually all boiling configurations—capillary, pool, falling-film, channel flow, microchannel, jet, and spray boiling—across a wide range of working fluids [1–9]. Each configuration offers distinct advantages depending on the application. Among them, pool boiling stands out as one of the most efficient and

* Corresponding author.
E-mail address: mudawar@ecn.purdue.edu (I. Mudawar).
URL: https://engineering.purdue.edu/mudawar (I. Mudawar).

https://doi.org/10.1016/j.ijheatmasstransfer.2026.128625
Received 21 November 2025; Received in revised form 28 February 2026; Accepted 2 March 2026
Available online 10 March 2026

Nomenclature

Abbreviations

CHF	Critical heat flux
FB	Film boiling
HTC	Heat transfer coefficient
LAr	Liquid Argon
LCH_4	Liquid methane
LHe	Liquid helium
LH_2	Liquid hydrogen
LN_2	Liquid nitrogen
LO_2	Liquid oxygen
MAE	Mean absolute error
MHF	Minimum heat flux
NASA	National Aeronautics and Space Administration
NB	Nucleate boiling
NC	Natural convection
NIST	National Institute of Standards and Technology
ONB	Onset of nucleate boiling
PU-BTPFL	Purdue University Boiling and Two-Phase Flow Laboratory
TB	Transition boiling
C	Coefficient of natural convection correlation [dimensionless]
c_p	Specific heat at constant pressure [J.kg^{-1}.K^{-1}]
F	Multiplier function in correlation accounting for different effects
g	Earth gravitational acceleration [9.81 m. s^{-2}]
h	Heat transfer coefficient [W.m^{-2}.K^{-1}]
h_{fg}	Latent heat of vaporization [J.kg^{-1}]
k	Thermal conductivity [W.m^{-1}.K^{-1}]
L_b	Laplace constant or bubble length [m]; $L_b = \sqrt{\frac{\sigma}{g(\rho_f-\rho_g)}}$
L_c	Characteristic length of heating surface; minimum dimension of heating surface (length or width) [m]
m	Empirical exponent in surface multiplier function
n	Exponent in natural convection correlation [dimensionless]; number of sampling points in surface profile [dimensionless]
Nu	Nusselt number [dimensionless]
p	Pressure [N. m^{-2}]
p^*	Reduced pressure; $p^* = \frac{p}{p_c}$ [dimensionless]
p_c	Critical pressure [N. m^{-2}]
p_i	Local height in surface profile [mm]
Pr	Prandtl number [dimensionless]
q''	Heat flux [W. m^{-2}]
R_a	Arithmetic mean surface roughness [μm]
Ra_g	Rayleigh number for film boiling based on bubble length L_b [dimensionless]
Ra_L	Rayleigh number for natural convection based on characteristic length L_c [dimensionless]
R_z	Average peak-to-valley height of surface roughness [mm]
T	Temperature [K]
T_c	Critical temperature [K]
T_f	Pool liquid temperature [K]
T_{sat}	Saturation temperature of fluid [K]
ΔT_{sat}	Wall superheat [K]; $\Delta T_{sat} = T_w - T_{sat}$
ΔT_{sub}	Liquid subcooling [K]; $\Delta T_{sub} = T_{sat} - T_f$
v_i	Local valley depth in surface profile [mm]
x	Planar coordinate in surface profile [mm]
y_i	Local height in surface profile [mm]

Greek symbols

α	Percentage of predictions within ±30 % of the data
b	Percentage of predictions within ±50 % of the data
θ	Orientation angle of heating surface [°]
λ_d	Taylor's most dangerous wavelength [m]; $\lambda_d = 2\pi\sqrt{3}\sqrt{\frac{\sigma}{g(\rho_f-\rho_g)}}$
μ	Dynamic viscosity [Pa.s]
ρ	Density [kg.m^{-3}]
σ	Surface tension [N.m^{-1}]
σ_b	Stefan-Boltzmann constant [5.67×10^{-8} W/m^2.K^4]
φ	Weighting function used in transition boiling correlation [dimensionless]

Subscripts

CHF	Critical heat flux
Cu	Based on copper
Exp	Experimental (measured)
f	Saturated liquid
fb	Film boiling
g	Saturated vapor
l	Single-phase liquid
M	Based on surface material
min	Minimum heat flux
nb	Nucleate boiling
nc	Natural convection
Pred	Predicted
R	Based on surface roughness
r	Radiation
S	Based on heater size
sat	Saturation
sub	Subcooling
tb	Transition boiling
w	Heating wall
θ	Based on surface orientation angle

practical cooling mechanisms due to its inherently high heat transfer coefficients, compact and simple design, low cost, and passive operation.

Over the past several decades, extensive research has been dedicated to elucidating the mechanisms governing pool boiling across a broad spectrum of thermodynamic and geometric conditions. These efforts have yielded numerous empirical and semi-empirical correlations capable of predicting boiling heat transfer performance with reasonable accuracy for a wide range of engineering applications. However, most existing predictive tools were developed for fluids operating near ambient temperatures—such as water, refrigerants, and dielectric coolants—and therefore have limited applicability under cryogenic conditions. Emerging technologies in cryogenics, superconductivity, and aerospace increasingly rely on fluids such as liquid nitrogen (LN_2), liquid hydrogen (LH_2), and liquid oxygen (LO_2), which operate at extremely low temperatures. These cryogenic fluids exhibit drastically different thermophysical and interfacial characteristics compared to conventional fluids; properties such as surface tension, viscosity, and density can differ by orders of magnitude. For example, at atmospheric pressure, the surface tension of water at 373 K is 58.9 mN/m, whereas that of LH_2 is about 1.9117 mN/m [10]. Similarly, the dynamic viscosity (m_f) of water is roughly 281 μPa·s at 373 K, compared to 13.5 μPa·s for LH_2 at 20.4 K [10], while the density ratio (ρ_f/ρ_g) is significantly larger for cryogens than for water. These substantial differences directly influence bubble dynamics, microlayer behaviour, and instability mechanisms. As a result, correlations calibrated for ambient-temperature fluids often produce substantial prediction errors when applied to cryogenic boiling, underscoring the urgent need for predictive tools that

explicitly capture the unique physics governing heat transfer in cryogenic pool boiling.

The overall performance of a pool boiling system is typically characterized by the *pool boiling curve*, which describes the relationship between wall superheat and heat flux. This curve comprises several distinct regimes and transition points—natural convection (NC), onset of nucleate boiling (ONB), nucleate boiling (NB), critical heat flux (CHF), transition boiling (TB), minimum heat flux (MHF), and film boiling (FB)—each governed by different physical mechanisms and dominant heat transfer processes. For example, NC is primarily driven by buoyancy-induced motion resulting from density gradients; NB involves complex bubble nucleation, growth, and departure dynamics; TB is characterized by unstable interactions between vapor and liquid phases; and FB is dominated by the formation of a stable vapor film. These fundamentally different mechanisms make it exceedingly difficult to develop a single theoretical or empirical model capable of accurately representing all boiling regimes and their transitions. To address this challenge, researchers have traditionally formulated separate regime-specific correlations, each tailored to a particular boiling regime. PU-BTPFL, in collaboration with NASA Glenn Research Center, has been at the forefront of these efforts. Their joint studies have consolidated an extensive cryogenic boiling database and developed updated correlations for individual regimes, including NB [11], CHF [12,13], TB [14], MHF [15], and FB [16]. These studies markedly improved the predictive accuracy of existing models and correlations, particularly for cryogenic fluids. More recently, this collaboration introduced a unified methodology for constructing a continuous boiling curve by combining these regime-specific correlations using a smooth blending function between the MHF and FB regimes [17]. This approach represented a major advancement toward achieving a complete and physically consistent description of the boiling process. However, that earlier work was primarily confined to saturated, steady-state conditions on flat surfaces with horizontal and vertical orientations. The correlations did not account for several key factors—such as liquid subcooling, heated surface material, heater size, orientation angle, and surface roughness—all of which are known to strongly influence boiling behaviour and therefore warrant further investigation [18].

Despite the substantial progress achieved to date, a critical gap remains in the existing literature—namely, the lack of generalized correlations capable of accurately capturing the combined effects of operational and surface parameters. Addressing this limitation requires a systematic and physically consistent framework that incorporates these additional influencing factors into the regime-specific correlations developed previously. Building on the strong foundation established through prior PU-BTPFL–NASA collaborations, the present study seeks to close this gap by developing an enhanced and comprehensive predictive methodology for cryogenic pool boiling. The proposed framework extends earlier correlations to explicitly account for the effects of subcooling, heated surface material, heater size, orientation, and surface roughness, thereby enabling accurate predictions over a substantially broader range of operating conditions. This advancement is expected to markedly improve the design, safety, and performance of cryogenic thermal management systems.

1.2. Objectives of the present study

The present study builds upon foundational work developed through an ongoing collaboration between PU-BTPFL and NASA Glenn Research Center, initiated in 2018. This joint effort was established to address the lack of reliable, cryogen-specific heat transfer correlations for pool boiling across a broad range of operating conditions. The collaboration has since resulted in the consolidation of an extensive cryogenic boiling database and the development of regime-specific correlations for saturated, steady-state pool boiling under terrestrial gravity. Expanding on this foundation, the current work aims to enhance the generality and applicability of the developed framework by systematically integrating additional physical parameters (discussed above).

The specific objectives of this study are as follows:

i. Utilize the previously compiled cryogenic boiling databases to systematically evaluate the effects of subcooling, heated surface material, surface size, orientation, and surface roughness on heat transfer performance across all boiling regimes (NB, TB, and FB) and transition points (CHF and MHF) for flat surfaces.
ii. Develop scaling factors for different effects and update the previously developed correlations to explicitly incorporate the effects of subcooling, surface material, size, orientation, and roughness.

In summary, this study represents a significant advancement in predictive modeling of cryogenic pool boiling on flat surfaces by systematically incorporating key operational and surface effects. The resulting framework offers a robust and reliable foundation for the design and performance evaluation of cryogenic thermal systems across a broad range of conditions.

2. New updated universal correlations for cryogenic pool boiling

2.1. Background

During the authors' previous studies [11–16], a set of 'baseline' cryogenic pool boiling correlations was developed to enable construction of a continuous boiling curve under saturated conditions. This framework marked a significant advancement in the understanding of cryogenic pool boiling, as it systematically incorporated the effects of pressure, wall heat flux, surface orientation (limited to FB and CHF), and cryogen-specific properties. This effort established a robust foundation for predicting cryogenic boiling behaviour over a wide range of operating conditions in terrestrial gravity. However, in practical applications, pool boiling systems are rarely confined to ideal saturated conditions. Several additional factors, such as subcooling, heated surface material, surface size, orientation, and roughness, can exert significant influence on the various boiling regimes and their transition points. Building upon the baseline cryogenic pool boiling correlations, the present study introduces an extended framework that systematically incorporates these effects.

Before examining in detail, the influence of each parameter on the different boiling regimes, it is important to highlight that the correlations developed in this study were based on a comprehensive pool boiling database compiled from a wide range of published sources. This universal database encompasses data obtained using various surface materials. To incorporate the effect of surface material, it was necessary to establish relationships for the thermal properties of each material as functions of temperature, since the database spans cryogenic fluids with boiling temperatures ranging from 4.2 K (lLHe at 0.1 MPa) to 187 K (LCH_4 at 4.5 MPa) [10]. However, due to limited availability of temperature-dependent thermal property data for some materials, only those surfaces for which reliable thermal conductivity data could be obtained were retained in the analysis. These include copper, platinum, aluminum, and stainless steel, with their temperature-dependent properties sourced from the NIST database [10]. Fig. 1 shows the variation in thermal conductivity with temperature from 4 K to 200 K, which was deemed sufficient for the present study.

In the following sections, each boiling regime and transition points will be examined individually, with detailed discussion of the influence of the aforementioned parameters. For clarity and ease of application, the units associated with each parameter are explicitly provided alongside the corresponding correlation. This approach is intended to assist the reader in correctly using the newly developed correlations and to prevent unit-related errors, an issue the authors frequently encountered while reviewing existing literature.

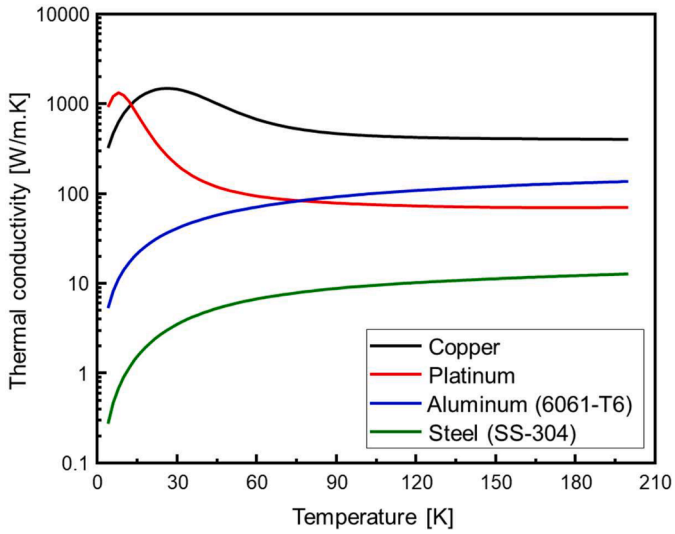

Fig. 1. Variation of thermal conductivity of metals with temperature (taken from NIST database [10]).

2.2. Natural convection (NC)

As noted in our previous study [17], no new correlation was developed for this regime, as it represents non-boiling behaviour and existing correlations for room-temperature fluids are applicable to cryogenic fluids as well (Wang et al. [19]). For the sake of completeness, the correlation used for NC regime is provided in [20].

$$Nu_{nc} = \frac{h_{nc}\, L_c}{k_l} = C\, Ra_L^n \tag{1}$$

Here, h_{nc} is the NC heat transfer coefficient [W.m^{-2}·K^{-1}], L_c is the minimum characteristic dimension of the heating surface (length or width, whichever is smaller) [m], Ra_L is the Rayleigh number based on L_c, and k_l is the thermal conductivity of the single-phase liquid [W.m^{-1}·K^{-1}]. The values of the empirical constants C and n depend on the flow regime (laminar or turbulent) and the orientation of the heated surface, as summarized in Table 1 based on references [21–24].

Ra_L in Eq. (1) is defined as

$$Ra_L = \frac{L_c^3\, \rho_l\, (\rho_l - \rho_{lw})\, g}{\mu_l^2} \left(\frac{\mu_l\, c_{pl}}{k_l}\right) \tag{2}$$

Here, ρ_l is the density of the single-phase liquid evaluated at the bulk liquid temperature [kg.m^{-3}], and ρ_{lw} is the density of the single-phase liquid evaluated at the wall temperature [kg.m^{-3}]; μ_l is the dynamic viscosity of the liquid [Pa·s]; g is the Earth's gravitational acceleration [9.8 m.s^{-2}]; and c_{pl} is the specific heat of the liquid [J.kg^{-1}.K^{-1}].

Table 1
Summary of values of C and n in the natural convection correlation.

Orientation angle [°]	C	n	Validity Range	Author(s) [ref. no.]
$\theta = 0°$	0.54	1/4	$10^4 \le Ra_L \le 10^7$, $Pr_l \ge 0.7$	Lloyd & Moran [21]
	0.15	1/3	$10^7 \le Ra_L \le 10^{11}$	Lloyd & Moran [21]
$\theta = 90°$	0.59	1/4	$10^4 \le Ra_L \le 10^9$	McAdams [22]
	0.10	1/3	$10^9 \le Ra_L \le 10^{13}$	Bayley [23]
$\theta = 180°$	0.52	1/5	$10^4 \le Ra_L \le 10^9$, $Pr_l \ge 0.7$	Radziemska & Lewandowski [24]

2.3. Nucleate boiling (NB)

Once the onset of nucleate boiling (ONB) conditions are met ($\Delta T = \Delta T_{ONB}$, $q'' = q''_{ONB}$), bubble nucleation initiates and intensifies through the nucleate boiling (NB) regime. This activity continues to escalate until it begins to subside as the system reaches CHF. In one of the authors' previous studies, a baseline correlation for the NB regime was developed [11], which was shown to be applicable across the entire cryogenic saturated-condition database, without segregation based on heater orientation, size, material, or surface roughness. Following is the form of the baseline correlation:

$$h_{nb} = 13.3\; q''^{0.665} (1 + 0.52\, p^*)^{4.7} Pr_f^{-1.09} \left[\frac{1 + 68 e^{20(p^* - 1.1)}}{1 + 0.0045\, e^{\left(q'' \times\ 10^{-5}\right)}}\right] \tag{3}$$

where h_{nb} is the NB HTC [W.m^{-2}.K^{-1}], p^* the reduced pressure (p/p_c), q'' the heat flux provided to the system [W.m^{-2}], and Pr_f the liquid Prandtl number. Details concerning both the development of this correlation and its predictive performance for different cryogens are provided in [11].

In the present study, an extensive analysis of cryogenic fluids databases was conducted to investigate the effects of the aforementioned parameters. As an initial screening step, data corresponding to heater materials other than copper, platinum, aluminum, and steel were excluded due to the lack of available temperature-dependent thermal property data for those materials. This filtering reduced the dataset from an initial 2908 data points to 2285. In the sections that follow, the influence of each parameter on the relevant pool boiling regime or transition point is systematically examined, and a corresponding multiplier is proposed to account for its effect.

2.3.1. Effects of surface roughness

In evaluating the influence of boiling surface roughness on the NB HTC, it was found that literature data exhibit substantial inconsistency in both measurement methodology and terminology. This inconsistency arises primarily from the broad use of different surface roughness parameters across various engineering disciplines. To illustrate the extent of this variability, Gadelmawla et al. [25] compiled and analysed 59 different definitions and mathematical formulations of surface roughness parameters, underscoring the complexity of roughness characterization. Building on this, Cai et al. [26] presented a comparative overview of common surface roughness metrics relevant to heat transfer applications, including the arithmetic mean roughness (R_a) and the average peak-to-valley height (R_z), along with their standardized definitions. A representative surface roughness profile, along with the definitions of key parameters, is shown in Fig. 2.

Although R_z is physically more representative of surface features that influence boiling behaviour, its values are sparsely reported in the compiled cryogenic pool boiling database. In contrast, R_a is the most frequently cited metric across the dataset. It is important to note that R_a and R_z quantify fundamentally different aspects of surface texture, and no universally accepted conversion exists between them. Nonetheless, to enable consistent analysis and incorporation of surface roughness effects into the NB correlation, approximate empirical relationships available in the literature were reviewed [26]. Based on the insights from the literature and the current database, the following conversion was adopted in the present study:

$$R_a \approx \frac{1}{4} R_z \tag{4}$$

It should be noted that this conversion is totally empirical in nature and is based on the current database. This conversion enabled the integration of otherwise incompatible surface roughness data, thereby facilitating the development of a unified correlation. Following the standardization of roughness parameters, the influence of surface roughness on NB performance was systematically investigated. It was

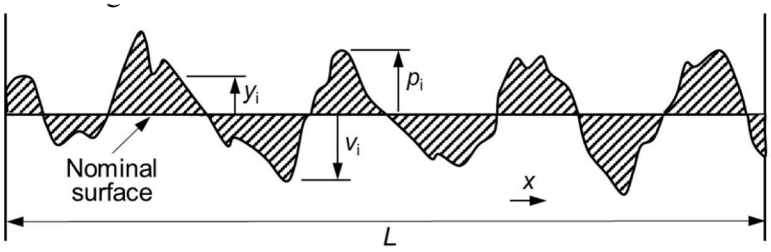

$$R_a = \frac{1}{L}\int_0^L |y_i|\,dx = \frac{1}{n}\sum_{i=1}^{n}|y_i|$$

$$R_z = \frac{1}{n}\left(\sum_{i=1}^{n} p_i - \sum_{i=1}^{n} v_i\right)$$

y_i	Local surface height
p_i	Local peak height
v_i	Local valley depth ($v_i < 0$)
R_a	Arithmetic mean roughness
R_z	Average roughness height
n	Number of sampling points
L	Sampling length

Fig. 2. Surface roughness profile (adapted from Cai et al. [26]), and definition of key statistical parameters [25].

found that for surfaces with R_a⟨ 0.1 μm, the effect of roughness on the NB HTC diminished substantially, suggesting that these surfaces could be reasonably classified as smooth. In contrast, surfaces with $R_a > 0.1$ μm exhibited noticeable enhancement in nucleate boiling performance and were thus categorized as rough. When the baseline nucleate boiling correlation, originally developed without accounting for surface roughness, was applied to the complete dataset, very good agreement was observed for smooth surfaces. However, for rough surfaces, a consistent underprediction of the HTC was evident, as shown in Figs. 3a and 3b The mean absolute error (MAE) for the rough surface data was found to be 47.68 %, indicating a significant deviation from the baseline predictions and clearly demonstrating the need for a correction factor or multiplier to incorporate the effects of surface roughness in the NB regime. It should be noted that there is limited information on roughness available in the literature, as can be seen from Fig. 3b

Fig. 4 further illustrates the influence of surface roughness on the NB HTC for LHe data [27]. A substantial enhancement in NB HTC is observed for rough surfaces. However, analysis of the broader database indicates that this enhancement approaches an asymptotic limit beyond a certain roughness level [28]. This behaviour can be attributed to a saturation of effective nucleation-site activity, whereby further increase in surface roughness does not introduce additional active cavities and thus the HTC remains asymptotic in nature. Additionally, variations in surface roughness were found to have negligible influence within the smooth regime [27]. Moreover, Fig. 3(b) shows that the LN_2 data are well predicted by the correlation and may initially appear to require no modification. However, closer examination of the database reveals that this agreement results from the simultaneous influence of two opposing effects: the lower thermal conductivity of aluminium reduces the predicted HTC, while surface roughness enhances it. When both effects are applied together, their compensating influences yield predictions that remain close to the experimental data, underscoring the importance of accounting for interacting parameters within a unified framework.

To accommodate these trends, a roughness multiplier function was developed to (i) converge to unity for $R_a < 0.1$ μm, (ii) increase gradually with surface roughness, and (iii) asymptotically approach a maximum value of 2.5 for $R_a > 0.5$ μm. It is important to note that the upper limit of this function is not derived from a theoretical basis, but rather reflects the range of available data and the need for a simple, practical correlation form. Based on these considerations, the following multiplier function is proposed for incorporation into the baseline NB correlation to account for surface roughness effects:

$$F_{R,\,nb} = 1 + \frac{1.5}{1 + e^{-30(R_a - 0.32)}} \tag{5}$$

where R_a is expressed in μm. Predictions incorporating this surface roughness multiplier will be presented in a later section after all other effects have been included. However, it should be noted that the updated correlation reduced the MAE of the rough surface data from 47.68 % to 22.43 %

2.3.2. *Effects of heated surface material*

Since heat transfer in the NB regime is strongly influenced by conduction within the heater surface, the thermal conductivity of the boiling surface must be accounted for through a material-based multiplier. The authors' previously developed NB correlation [11] was found to perform well for copper surfaces; therefore, copper was selected as the reference material. The effect of surface material was incorporated through the ratio of the wall thermal conductivity to that of copper. Because copper has the highest thermal conductivity among commonly used boiling surfaces, the material-based multiplier is expected to be less than unity for other materials. Accordingly, the following functional form was adopted, with the exponent determined from the experimental database:

$$F_{M,\,nb} = \left(\frac{k_w}{k_{Cu}}\right)^m \tag{6}$$

Here, k_w is the thermal conductivity of the wall material, and k_{Cu} is the thermal conductivity of copper, both evaluated at the saturation temperature of the working fluid. Comparative analysis of data across different surface materials revealed that the influence of thermal conductivity is more pronounced for rough surfaces [28] than for smooth ones [28,29], as illustrated in Fig. 5. As a result, a single constant exponent m could not adequately capture the behaviour for both surface categories. Through database optimization, the best-fit exponent values were determined to be $m = 0.02$ for smooth surfaces ($R_a \leq 0.1$ μm) and $m = 0.15$ for rough surfaces (Ra > 0.1 μm). Predictions incorporating

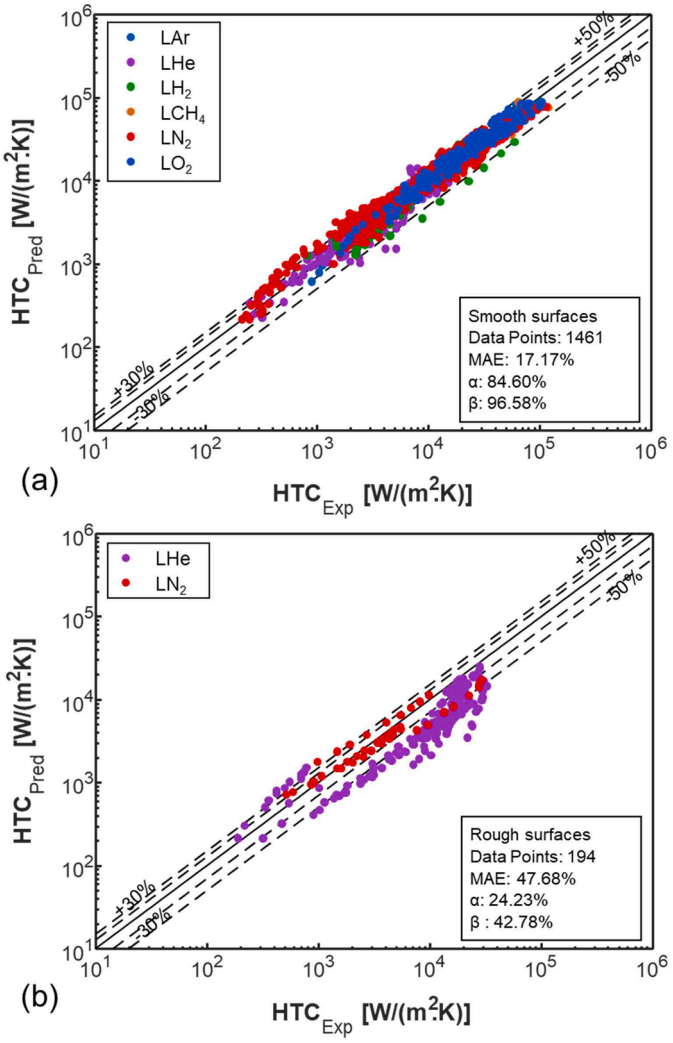

Fig. 3. Predictions of the baseline NB HTC correlation [11] against data for (a) smooth surfaces and (b) rough surfaces. (Data taken from Ahmad et al. [11] NB consolidated database).

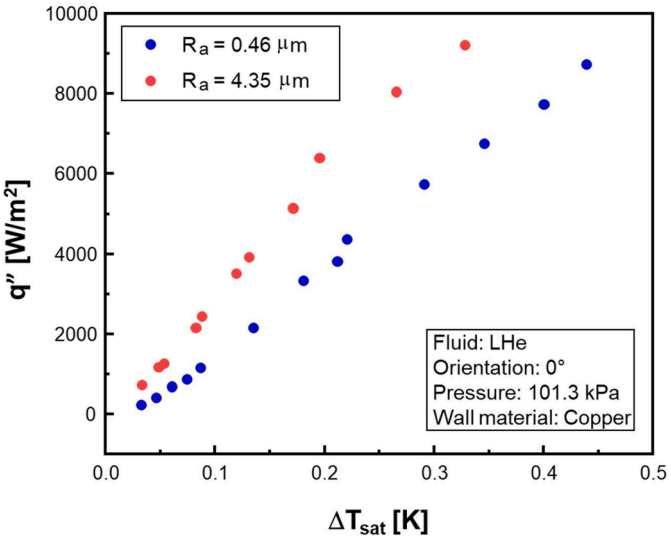

Fig. 4. NB heat flux versus wall superheat for LHe for rough surfaces with different R_a values. (Data taken from [27]).

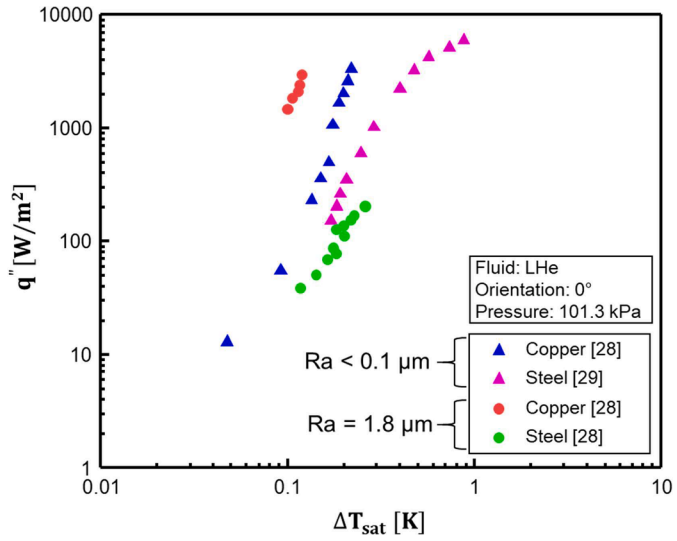

Fig. 5. NB heat flux versus wall superheat for LHe comparing the effect of thermal conductivity for smooth and rough surfaces. (Data taken from [28,29]).

the material multiplier from Eq. (6) will be presented in a subsequent section following the integration of all additional effects.

2.3.3. *Effects of surface orientation*

The effect of surface orientation on the NB HTC remains inconclusive. While some studies have reported a measurable enhancement in HTC when transitioning from horizontal upward-facing to vertical orientations, others have found negligible or no discernible impact. Relevant details can be found in authors' prior NB paper [11]. Owing to these inconsistencies, surface orientation was initially excluded from the baseline NB correlation in our previous study. However, a deeper look into the database revealed that incorporating a surface orientation multiplier slightly reduced the overall MAE, suggesting that a majority of the data favors a positive correlation between surface orientation and HTC. Based on this observation, the following multiplier function is proposed to account for the influence of heated surface orientation:

$$F_{\theta,\ nb} = 1 + 0.04\ sin\theta \tag{7}$$

where θ is in degrees. It should be noted that this equation was developed for orientations from $\theta = 0^{\circ}$ to $\theta = 90^{\circ}$.

2.3.4. *Effects of subcooling*

According to most prior investigations, liquid subcooling has been found to exert a measurable influence on the NB HTC. However, the magnitude and nature of this influence vary across different cryogens. For instance, Figs. 6a and 6b illustrate the variation in boiling curves at different degrees of subcooling for liquid helium (LHe) [30] and liquid hydrogen (LH_2) [31], respectively. Notably, the effect of subcooling on LHe does not exhibit a monotonic trend, which appears inconsistent with the expected physical behaviour of subcooled boiling. This non-monotonicity may be attributed to three potential factors: (i) the inherently small bubble size in LHe may limit further reduction by subcooling; (ii) the extremely low saturation temperature of LHe complicates accurate measurement of wall superheat, particularly under subcooled conditions; and (iii) the data were digitized from published plots, introducing a higher likelihood of temperature inaccuracies at these very low values. Despite these limitations, the best overall fit to the subcooled data was achieved using the following multiplier function:

$$F_{sub,\ nb} = 1 + 1.3\left(\frac{\rho_f}{\rho_g}\right)^{0.4}\left(\frac{c_{p,f}\ \Delta T_{sub}}{h_{fg}}\right)^{3.5} \tag{8}$$

where ρ_f and ρ_g are the densities of the saturated liquid and saturated

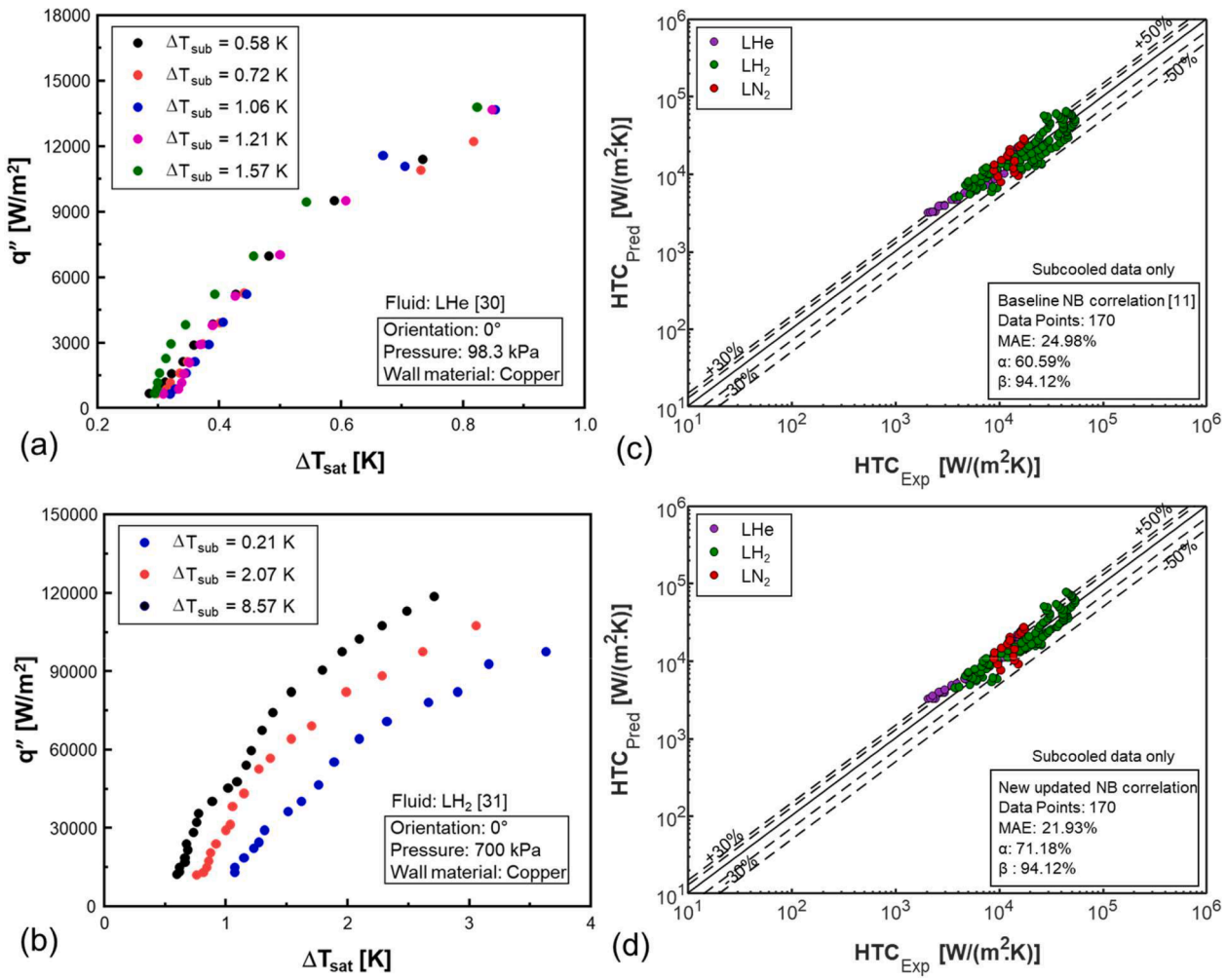

Fig. 6. NB heat flux versus wall superheat for different inlet subcoolings for (a) LHe and (b) LH_2, and Predictions of (c) baseline NB HTC [11] and (d) updated NB HTC for subcooled data from the cryogenic database. (Data taken from [30,31]).

vapor [kg.m^{-3}], respectively, both evaluated at the saturation pressure, $c_{p,f}$ is the specific heat capacity of the saturated liquid [J. kg^{-1}.K^{-1}], h_{fg} is the latent heat of vaporization [J. kg^{-1}], and ΔT_{sub} is the degree of subcooling [K]. As demonstrated in Fig. 6c and 6d, the application of this multiplier to the baseline NB correlation yields improved predictions for subcooled data, reducing the MAE from 24.98 % to 21.93 %.

2.3.5. *Effect of heated surface size*

Analysis of the consolidated database for the NB regime revealed that heated surface length exerts some influence on NB behaviour. However, this influence was not consistent across all fluids and did not exhibit a clear monotonic trend. Efforts to incorporate this effect through a heated surface length multiplier led to an increase in the overall MAE of predictions. As a result, this parameter was excluded from the current correlation development. It is recommended that the effect of heated surface length on NB be investigated more thoroughly in a dedicated future study, where fluid-specific behaviours and interactions can be systematically evaluated.

2.3.6. *Final updated nucleate boiling correlation*

In the authors' previous study [11], a heat flux multiplier $\left(1+0.0045\ e^{\left(q''\times\ 10^{-5}\right)}\right)$ was introduced in the denominator of Eq. (3) to reduce MAE at higher heat fluxes in the NB regime. While effective, this multiplier introduced several complexities:

i. It rendered the correlation implicit.
ii. It performed well primarily for q''_{CHF} values below 800 kW.m^{-2}, which is suitable for cryogenic fluids; however, recent research increasingly targets higher q''_{CHF} values.
iii. The current form of the correlation may not be applicable to non-cryogenic fluids (e.g., water), where q''_{CHF} values are significantly higher.

To address these limitations, the multiplier was removed despite a modest increase in MAE (approximately 1–2 %). Incorporating this adjustment, along with the additional multipliers described earlier, a significantly improved predictive expression for NB HTC is developed. The updated correlation is given as:

$$\begin{aligned} h_{nb} \;=\; & 13.3\, q''^{\,0.665}\left(1+0.52\,p^*\right)^{4.7}\left(1+68\,e^{20(p^*-1.1)}\right) Pr_f^{-1.09} \\ & \times\left[1+1.3\left(\frac{\rho_f}{\rho_g}\right)^{0.4}\left(\frac{c_{p,f}\,\Delta T_{sub}}{h_{fg}}\right)^{3.5}\right] \\ & \times\left[1+\frac{1.5}{1+e^{-30(R_a-0.32)}}\right] nonumber \\ & \times\left[\left(\frac{k_w}{k_{Cu}}\right)^{m}\right] \\ & \times\left[1+0.04\,\sin\theta\right] \end{aligned} \tag{9}$$

where

$m = 0.02$ for smooth surfaces ($R_a \leq 0.1$ μm)
$m = 0.15$ for rough surfaces (Ra > 0.1 μm)

This updated correlation explicitly accounts for the effects of surface roughness, heater size, material thermal conductivity, surface orientation, and liquid subcooling. The only remaining influential parameter not yet incorporated is gravity, which is expected to be incorporated upon acquisition of additional reduced gravity data from the authors' upcoming parabolic flight experiments. Fig. 7 presents a comparison between predictions from the original baseline NB HTC correlation (excluding the above factors) and those from the updated correlation (including all applicable multipliers). As evident from the figure, the inclusion of these multipliers has notably improved prediction accuracy, reducing the MAE from 20.75 % to 17.46 %. This improvement is particularly pronounced for data that were previously underpredicted by the baseline correlation especially for rough surfaces. Furthermore, the statistical performance parameters α and β have improved by approximately 6 %, underscoring the enhanced reliability and robustness of the updated correlation. It should be noted that among all these parametric effects, surface roughness was found to be one of the most influential.

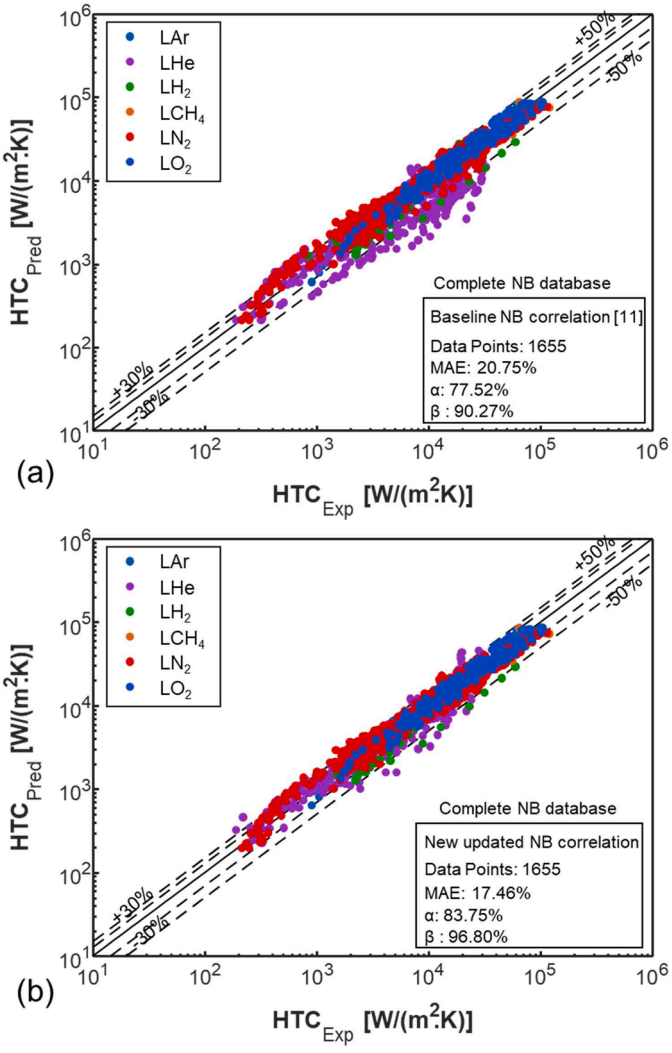

Fig. 7. Predictions of (a) baseline NB HTC and (b) updated NB HTC for complete cryogenic database. (Data taken from Ahmad et al. [11] NB consolidated database).

2.4. Onset of nucleate boiling (ONB) point

The ONB is defined as the condition at which the first vapor bubble forms on the heated surface. This point is typically characterized by a specific heat flux, q''_{ONB}, and a corresponding wall superheat, ΔT_{ONB}. Although, in theory, the ONB point lies on the NC curve, practical implementation often necessitates a blending function to ensure a smooth transition between the NC and NB regimes, thereby avoiding discontinuities in the boiling curve. However, the development of a reliable ONB correlation for cryogenic fluids has been impeded by two key challenges identified during an extensive literature review: (i) the limited availability of ONB data across different cryogens, and (ii) the inherently low magnitudes of q''_{ONB} and ΔT_{ONB}, which are often within the margin of experimental measurement uncertainty. To overcome these limitations, the present study defines the ONB point as the intersection of the NC and NB correlations, effectively using the condition: $(\Delta T_{nc},\ q''_{nc}) = (\Delta T_{nb}, q''_{nb})$. This approach is consistent with the methodology established in the authors' prior work [17], and no further modifications are introduced in this regard. Please note that this definition is a modeling approximation adopted for curve continuity rather than a direct physical ONB measurement.

2.5. Critical heat flux (q''_{CHF}) and wall temperature ($T_{w,CHF}$)

The CHF point is identified on the boiling curve by its associated heat flux, q''_{CHF}, and wall superheat, ΔT_{CHF}. A baseline correlation for q''_{CHF} was developed by Patel et al. [12] at the PU-BTPFL and is expressed as:

$$q''_{CHF} = \left[0.16 - 0.104\ (p^*)^{10}\right] \times \left[1 - 0.004\ (p^*)\theta\ \right] \left|\cos\left(\frac{88}{180}\theta\right)\right|^{0.364} \times \left[1 + 0.16\left(\frac{c_{p,f}\ \Delta T_{sub}}{h_{fg}}\right)\right] \times \left[\rho_g\ h_{fg}\left(\frac{\sigma\ g\ (\rho_f - \rho_g)}{\rho_g^2}\right)^{\frac{1}{4}}\right] \times \left[\frac{a}{g}\right]^{0.17} \tag{10}$$

where p^* is the reduced pressure (p/p_c), θ is the orientation angle of the heating surface [°], σ is the surface tension of the fluid [N·m^{-1}], a is the gravitational acceleration [m·s^{-2}], and g is the standard Earth gravitational acceleration [m·s^{-2}]. This correlation accounts for the effects of subcooling, surface orientation, and gravitational acceleration. However, it does not incorporate the influences of heated surface material, size, or roughness. To address these additional parameters, PU-BTPFL recently conducted an experimental investigation of cryogenic CHF, which includes a comprehensive evaluation of surface-related effects [13]. For completeness, a brief overview of the newly developed CHF correlation and the additional parameters considered is provided below.

2.5.1. Effects of surface roughness on q''_{CHF}

The effect of surface roughness on CHF remains a topic of ongoing debate within the heat transfer community. While several studies have reported a positive correlation between surface roughness and CHF, others have observed negligible or inconsistent influence. For example, Ferjancic and Golobic [32] investigated the effect of surface roughness on the CHF of water under saturated conditions and reported a direct relationship—CHF increased with increasing surface roughness. Similarly, Theofanous and Dinh [33] concluded that CHF is enhanced by a higher density of nucleation sites, which are often influenced by the surface's roughness characteristics. Fan et al. [34] also observed a significant enhancement in the CHF of HFE-7100 with increased surface roughness, reinforcing the hypothesis that surface microstructure can promote early rewetting and delay film formation.

In contrast, other researchers have reported differing outcomes regarding the influence of surface roughness on CHF. O'Hanley et al. [35] observed no significant effect of surface roughness on CHF across a range of working fluids and surface preparations. Similarly, Berenson

[36], in experiments conducted with n-pentane, concluded that CHF remained largely unaffected by variations in surface roughness. Furthermore, Alvariño et al. [37] noted that while increasing surface roughness initially enhances CHF, this effect tends to plateau beyond a certain threshold, suggesting a diminishing return at higher roughness levels.

Keeping in view the aforementioned discussion, the existing experimental evidence does not reveal a consistent or universally applicable dependence of CHF on surface roughness across fluids and surface types. Consequently, based on the available data and literature, the development of a reliable and general multiplier function to account for surface roughness effects on CHF cannot be proposed at this time.

2.5.2. Effect of surface material on q''_{CHF}

As discussed previously in the context of NB, higher thermal conductivity of the heated surface improves the NB HTC by promoting more uniform lateral heat distribution. This advantageous effect persists throughout the NB regime and extends up to the CHF point. Surfaces with high thermal conductivity such as copper tend to maintain lower wall temperatures and delay the onset of CHF by effectively redistributing heat from localized hot spots to cooler regions. In contrast, surfaces with lower thermal conductivity, such as stainless steel, are less effective at lateral heat conduction, resulting in steeper surface temperature gradients and earlier CHF onset. This trend is supported by experimental data for liquid helium (LHe), as shown in Fig. 8. The data, sourced from the database compiled by Patel et al. [12], clearly show that copper consistently yields the highest CHF, followed by platinum and then stainless steel, under identical operating conditions (atmospheric pressure). It is important to note that the horizontal axis in Fig. 8 is represented by discrete data sets, as the wall superheat at CHF was not reported by some sources, precluding a continuous representation.

2.5.3. Effect of heated surface size on q''_{CHF}

Fig. 8 highlights the importance of incorporating a multiplier to account for the effect of surface material on CHF. It was initially anticipated that including thermal conductivity alone would resolve the observed discrepancies. However, Lienhard et al. [38] noted that the length of the heated surface influences CHF when it is less than approximately three times Taylor's 'most dangerous wavelength,' λ_d. Specifically, smaller heaters promote enhanced peripheral liquid recirculation, which disrupts vapor instabilities and delays CHF onset, allowing for higher heat flux limits. To assess the impact of heater size on CHF, data from the consolidated database by Patel et al. [12] were combined with results from Foster et al. [13] and plotted against the nondimensionalized heater length L_c/λ_d, as shown in Fig. 9, alongside predictions from the CHF correlation proposed by Patel et al. [12]. The results reveal a decreasing trend in CHF with increasing heater size, which levels off for surfaces with characteristic lengths greater than approximately $3\lambda_d$, a trend consistent with the earlier observations of Lienhard et al. [38]. Notice that the correlation by Patel et al. [12] does not capture this behaviour, as it assumes a constant CHF value regardless of heater size. To address this limitation, Foster et al. [13] introduced a correction multiplier to account for both heated surface material and size effects. The predictions from their updated correlation, plotted in Fig. 9, demonstrate good agreement with the CHF data across a range of nondimensional heater lengths. Their correlation effectively captures the influence of both parameters, providing a more comprehensive predictive capability for CHF behaviour in cryogenic boiling systems.

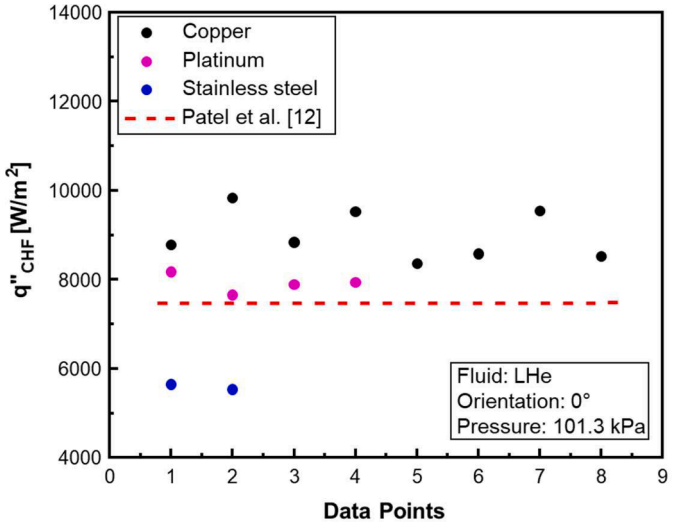

Fig. 8. CHF dependence on heated surface material for LHe. (Data taken from Patel et al. [12] consolidated database of CHF).

2.5.4. Final updated q''_{CHF} correlation

After incorporating the effects of heater size and surface material, Foster et al. [13] also revised the pressure-dependent term in the baseline CHF correlation to further reduce the MAE. This modification was guided by extensive analysis of the consolidated cryogenic CHF database and aimed at improving predictive accuracy across a broad range of operating pressures and cryogens. The final form of the updated correlation for q''_{CHF} is presented as follows:

$$
\begin{aligned}
q''_{CHF} &= \left[0.05\left(\frac{p}{p_c}\right)^{0.2} - 0.104\left(\frac{p}{p_c}\right)^{12} + 0.12\right] \\
&\times \left[1 - 0.004\left(\frac{p}{p_c}\right)\theta\right]\left|cos\left(\frac{88}{180}\,\theta\right)\right|^{0.364} \\
&\times \left[1 + 0.16\left(\frac{c_{p,f}\,\Delta T_{sub}}{h_{fg}}\right)\right] \\
&\times \left[\rho_g\, h_{fg}\left(\frac{\sigma\, g\, (\rho_f - \rho_g)}{\rho_g^2}\right)^{1/4}\right]\left[\frac{a}{g}\right]^{0.17} \\
&\times \left[e^{-1.7\left(\frac{L_c}{3\lambda_d}\right)^{-0.4}} + 1\right]\left[0.49\left(\frac{k_w}{k_f}\right)^{0.065}\right]
\end{aligned}
\tag{11}
$$

where k_f is the thermal conductivity of saturated liquid, k_w is the thermal

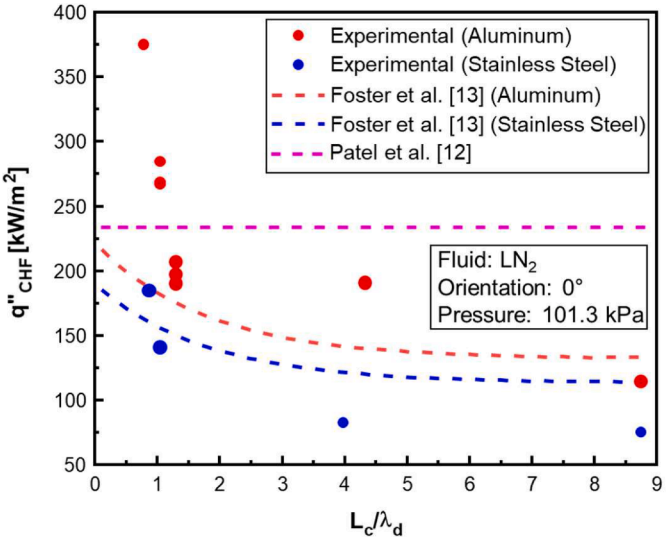

Fig. 9. Variation of CHF for LN_2 with heater characteristic length normalized by Taylor's most dangerous wavelength compared to predictions of correlations by Patel et al. [12] and Foster et al. [13]. (Data taken from the consolidated CHF database of Patel et al. [12] and Foster et al. [13]).

conductivity of the wall material evaluated at the saturation temperature of the working fluid, L_c is the minimum dimension of heated surface (length or width) [m], and λ_d is Taylor's most dangerous wavelength [m], which is given as:

$$\lambda_d = 2\pi\sqrt{3}\sqrt{\frac{\sigma}{g(\rho_f - \rho_g)}} \tag{12}$$

2.5.5. Calculation of ΔT_{CHF}

Since the CHF point requires two coordinates—heat flux at CHF (q''_{CHF}) and wall superheat at CHF (ΔT_{CHF})—to be represented on the boiling curve, the previously defined q''_{CHF} value is used in conjunction with the NB correlation to determine the corresponding ΔT_{CHF}. Specifically, ΔT_{CHF} is calculated by identifying the point on the NB curve at which the predicted heat flux matches q''_{CHF}. Mathematically, this can also be expressed as:

$$\Delta T_{CHF} = T_{w,CHF} - T_{sat} = \frac{q''_{CHF}}{h_{CHF}} \tag{13}$$

where h_{CHF} is the HTC at the CHF point, which is calculated by inserting Eq. (19) in Eq. (11).

$$h_{CHF} = h_{nb}\big|_{q''_{nb} = q''_{CHF}} \tag{14}$$

2.6. Minimum heat flux (q''_{min}) and wall temperature ($T_{w,min}$)

The MHF point represents the lower boundary between the transition boiling (TB) and film boiling (FB) regimes. To accurately locate this point on the boiling curve, two correlations are required: one for the minimum wall superheat (ΔT_{min}) and another for the corresponding heat flux (q''_{min}). These correlations are essential for generating a complete and continuous boiling curve. In the authors' previous study [15], baseline correlations were developed for both ΔT_{min} and q''_{min}, which showed strong agreement with experimental data, yielding a MAE of 9.05 % for clean surfaces without coatings or oxidation. However, these baseline correlations were primarily validated under moderate pressure conditions and were not extensively evaluated across the full pressure range approaching the critical point due to limited availability of high-pressure data in the literature.

2.6.1. Effects of pressure on $T_{w,min}$

In this section, the results of the previously published $T_{w,min}$ correlation [15] are evaluated across the full pressure range, as illustrated in Fig. 10. The baseline correlation predicts a predominantly increasing trend for LN_2 and LH_2, whereas a monotonically decreasing trend is observed for LHe. This apparent inconsistency is primarily attributed to the limited and non-overlapping pressure ranges over which experimental data are available. Specifically, LN_2 and LH_2 data are confined to low pressures ($p^* = 0.02$–0.15), while LHe data are available only at high pressures ($p^* = 0.44$–0.99). This lack of data continuity poses a major challenge in developing a unified correlation applicable across different cryogenic fluids. To address this limitation, an effort is made in this study to logically infer the expected trend of $T_{w,min}$ based on the following fundamental physical reasoning:

i. In the authors' previous study [14], it was demonstrated that the instabilities associated with both CHF and MHF exhibit notable similarities. This observation has prompted several researchers to propose analogous formulations for these two parameters. For instance, the q''_{min} correlations proposed by Cai et al. [26] and Morozov et al. [39] adopt the same underlying functional form as the q''_{CHF} correlations developed by Kutateladze [40], Zuber et al. [41], and Mudawar et al. [42], differing primarily in the numerical coefficients or applied multipliers. Experimental investigations have consistently shown that both CHF and MHF increase with pressure in the low-pressure region, followed by a decline beyond a reduced pressure of approximately $p^* = 0.35$, with this decreasing trend continuing up to the critical point.

ii. Moreover, as shown in Fig. 11, $T_{w,min}$ is observed to increase with pressure for LN_2 and LH_2, while it decreases with pressure for LHe. This contrasting behaviour is primarily a consequence of the

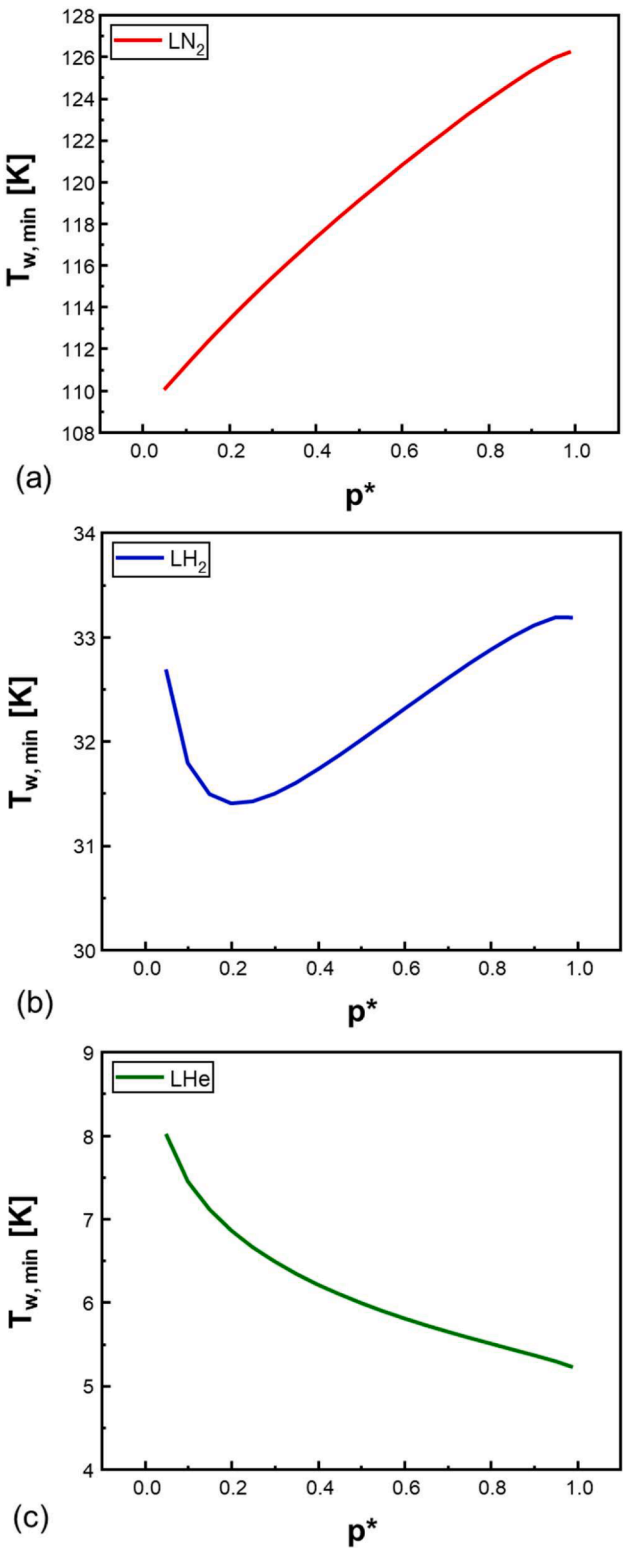

Fig. 10. Variation of minimum wall temperature with reduced pressure according to the baseline correlation [15] for (a) LN_2, (b) LH_2, and (c) LHe.

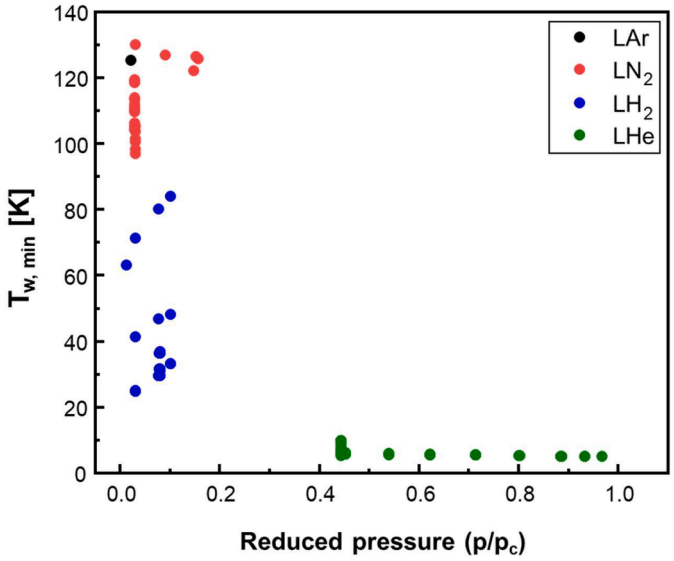

Fig. 11. Variation of minimum wall temperature with reduced pressure for different cryogens. (Data taken from Ahmad et al. [15] consolidated T_{min} database).

differing pressure ranges over which data are available for each fluid. However, when the data from all three fluids are considered collectively, a general trend becomes apparent: $T_{w,min}$ increases in the low-pressure region and decreases at higher pressures. This trend mirrors the well-established pressure dependence of CHF and MHF. Based on this observation, it is postulated that the pressure dependence of $T_{w,min}$ follows a similar pattern to that of CHF and MHF.

2.6.2. *Effects of surface material on* $T_{w,min}$ *and* q''_{min}

In addition to revealing the overall pressure-dependent trend, Fig. 11 shows that the LH_2 data form three distinct clusters. Although each cluster exhibits a similar pressure-dependent trend, their $T_{w,min}$ values differ significantly. A detailed examination reveals that these clusters correspond to different surface materials. This observation underscores the important role of surface thermal conductivity in influencing the MHF point, analogous to its previously established effect on CHF. To quantitatively account for the influence of surface thermal conductivity on both $T_{w,min}$ and q''_{min}, a material correction factor, $F_{M,min}$, is introduced. This factor is based on the ratio of the thermal conductivity of the heater material to that of copper, and is expressed as:

$$F_{M,\,min} = \left(\frac{k_{Cu}}{1 + k_w}\right)^{0.07} \tag{15}$$

where k_{Cu} is the thermal conductivity of copper [W/m.K], and k_w is the thermal conductivity of the heated wall material [W/m.K], both evaluated at the saturation temperature of the working fluid.

2.6.3. *Final updated correlation for* $T_{w,min}$

In the baseline correlation, recommendations from the literature were followed to represent the pressure dependence solely through the use of saturation temperature. However, as demonstrated in Fig. 10, relying exclusively on saturation temperature proved inadequate for accurately capturing the observed pressure trends described in the preceding section. To overcome this limitation, a pressure-dependent function is introduced into the correlation to more effectively account for the influence of system pressure. By incorporating both thermal conductivity effects and explicit pressure dependence, a more robust and physically representative formulation for $T_{w,min}$ is developed:

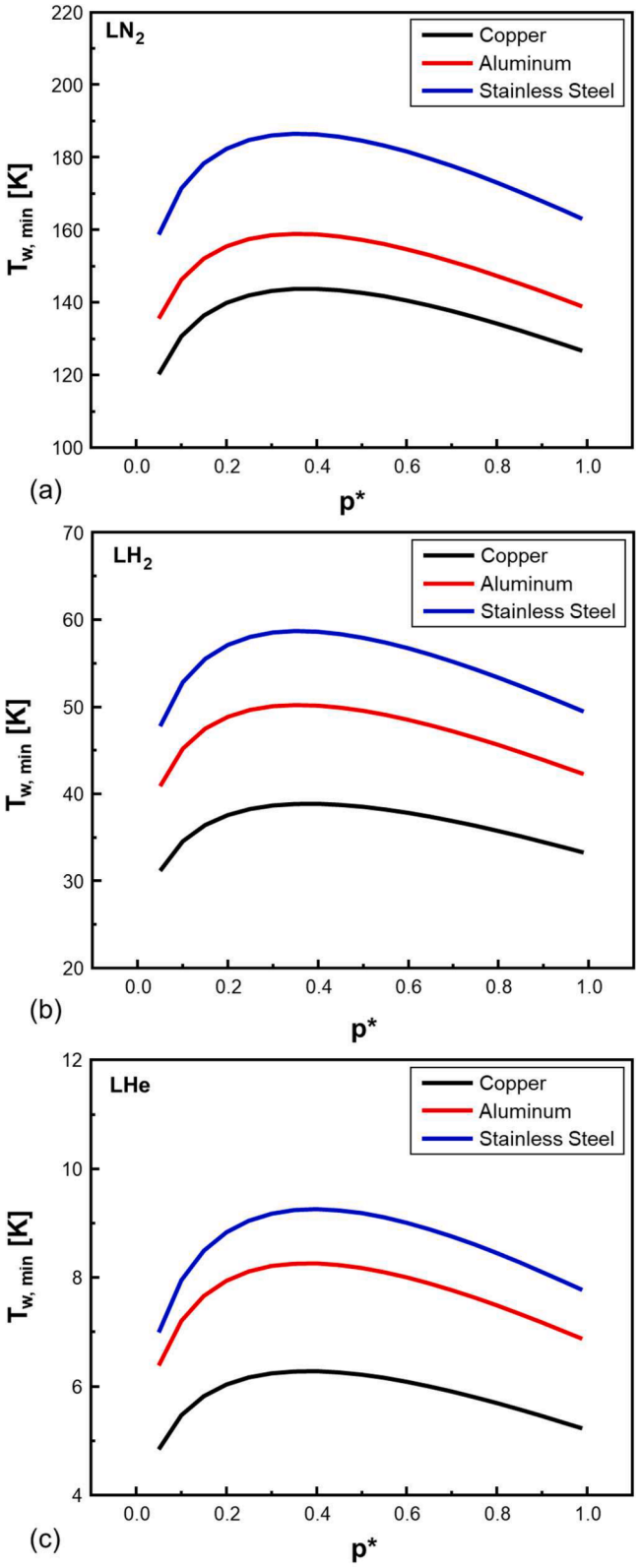

Fig. 12. Variation of $T_{w,min}$ with reduced pressure for different surface materials predicted according to newly modified correlation for (a) LN_2, (b) LH_2, and (c) LHe.

$$T_{w,min} = \left[T_{sat} + 1.6\ (T_c - T_{sat})\left(0.15 + 1.74\left(\frac{p}{p_c}\right)^{0.5}\right)\right]\left[\frac{k_{cu}}{1\ +\ k_w}\right]^{0.07} \tag{16}$$

This modified correlation enables improved prediction of $T_{w,min}$ across a broader range of operating pressures, surface materials, and cryogenic fluids. As illustrated in Fig. 12, the updated formulation exhibits significantly better agreement with experimental data over varying materials and pressure conditions. Nonetheless, the preceding analysis underscores the need for additional experimental studies spanning wider pressure ranges for multiple cryogens to further validate and refine the correlation. For application in the boiling curve, the corresponding minimum wall superheat, ΔT_{min}, can be calculated as:

$$\Delta T_{min} = T_{w,min} - T_{sat} \tag{17}$$

2.6.4. Effects of heater size on q''_{min}

Similar to CHF, the effect of heater size on the MHF point heat flux was also investigated, revealing a trend nearly identical to that observed for q''_{max}. As previously noted, Foster et al. [13] established that CHF is influenced by heater size when the minimum surface dimension, L_c, (width or diameter) is less than three times the Taylor most dangerous wavelength (λ_d). Analysis of the available MHF data revealed a comparable dependence, indicating that heater size similarly affects q''_{min} under these geometric constraints. This size effect is accounted for using the following multiplier, which adjusts the predicted q''_{min} based on the ratio L_c/λ_d:

$$F_{S,\ min} = 1 + 2.8\ e^{-0.36\left(\frac{L_c}{\lambda_d}\right)^2} \tag{18}$$

where L_c is in [m].

2.6.5. Effects of heater orientation on q''_{min}

During the formulation of the baseline correlations, the effect of surface orientation on the MHF point was initially found to be almost negligible. However, a more detailed analysis of the dataset across various orientations revealed that surface orientation does exert a minor influence on q''_{min}. Incorporating this subtle effect into the correlation allows for a reduction in MAE of the baseline prediction. This improvement is achieved through the application of the following orientation-based multiplier:

$$F_{\theta,\ min} = 1 + 0.2\sin\ (1.1\ \theta) \tag{19}$$

where θ is in degrees.

2.6.6. Effects of subcooling on MHF point

Due to the lack of available subcooled data for $T_{w,min}$, the development of a subcooling multiplier for this parameter could not be pursued. However, a very limited set of data points was identified for subcooled q''_{min}, based on which the following subcooling multiplier is proposed:

$$F_{sub,\ min} = 1 + 1.3\left(\frac{\rho_f}{\rho_g}\right)^{0.2}\left(\frac{c_{p,f}\ \Delta T_{sub}}{h_{fg}}\right) \tag{20}$$

It is important to note that the subcooling multiplier proposed for q''_{min} is developed based on a relatively limited number of experimental datapoints. Therefore, this effect should be explored further in future studies, and the multiplier should be updated based on the new data. The primary objective of this multiplier here is to capture the observed trend of increasing q''_{min} with subcooling rather than to provide a universally applicable correlation.

Given the incorporation of multiple correction multipliers and the modification of the $T_{w,min}$ correlation, which serves as a key input to the q''_{min} formulation, further adjustments are made to various exponents and coefficients to enhance predictive accuracy. These refinements culminated in the development of the following revised correlation for q''_{min}:

$$\begin{aligned} q''_{min} \ =\ & 0.0348 \quad \left[\frac{c_{p,\ g}\ k_g^2}{\mu_g}\rho_g\ g(\rho_f - \rho_g)\right]^{0.549} \left[0.414\ \left(\Delta T_{min,\ Cu}\right)^{0.399} - 0.112\right]^{3.1217} \\ & \times\left[1 + 1.3\left(\frac{\rho_f}{\rho_g}\right)^{0.2}\left(\frac{c_{p,f}\ \Delta T_{sub}}{h_{fg}}\right)\right][1 + 0.2\ \sin(1.1\ \theta)] \\ & \times\left[1 + 2.8\ e^{-0.36\left(\frac{L_c}{\lambda_d}\right)^2}\right]\left[\frac{k_{Cu}}{1 + k_w}\right]^{0.07} \end{aligned} \tag{21}$$

Here, $\Delta T_{min,\ Cu}$ denotes the wall superheat at the MHF point calculated for copper surfaces. The predictions of the revised q''_{min} correlation as a function of pressure for various surface materials are presented in Fig. 13. It is evident that the updated formulation effectively captures the pressure-dependent trend and accurately incorporates the influence of key parameters, most notably, surface thermal conductivity.

2.7. Transition boiling (TB)

Compared to the other boiling regimes, TB has received significantly less attention in the heat transfer literature. A comprehensive discussion on the limited number of existing correlations, their performance, and the underlying physics of the TB regime is presented in the authors' recent study [14]. In the same work, a new systematic method was proposed for determining the TB curve. First, the wall superheat in the TB region is given by:

$$\Delta T_{tb} = T_{w,tb} - T_{sat} = \Delta T_{CHF} + \varphi\ (\Delta T_{min} - \Delta T_{CHF}) \tag{22}$$

where ΔT_{tb} is the TB wall superheat [K], ΔT_{min} and ΔT_{CHF} are the wall superheats [K] corresponding to the MHF and CHF points, respectively (these can be calculated using Eqs. (17) and (13)), and φ is a weighting function that varies between 0 and 1 and depends on the relative position of the input heat flux within the TB region. The weighting function is defined as:

$$\varphi = \left|\left(\frac{q''_{tb}\ -\ q''_{CHF}}{q''_{min}\ -\ q''_{CHF}}\right)^{0.8}\right| \tag{23}$$

where q''_{tb} is the applied heat flux [W·m^{-2}] in the TB region, and q''_{CHF} and q''_{min} are the critical and minimum heat flux values calculated using Eqs. (11) and (21), respectively. The HTC in the TB region can then be expressed using the standard definition $h_{tb} = q''_{tb}/\Delta T_{tb}$, which yields

$$h_{tb} = \frac{q''_{tb}}{\left[\left(T_{w,CHF} - T_{sat}\right) + \left|\left(\frac{q''_{tb} - q''_{CHF}}{q''_{min} - q''_{CHF}}\right)^{0.8}\right| \left\{\left(T_{w,min} - T_{sat}\right) - \left(T_{w,CHF} - T_{sat}\right)\right\}\right]} \tag{24}$$

It should be noted that Eq. (24) is structurally identical to the equation used in the baseline study [14]. However, the TB regime is modified in the present work by virtue of the updated correlations for CHF and MHF, which directly influence the input parameters used in this formulation.

2.8. Film boiling (FB)

Film boiling (FB) is recognized as the highest temperature regime in pool boiling, wherein the high surface temperature causes bubble nucleation to completely subside and be replaced by the formation of a continuous vapor blanket. A detailed description of this regime and its characteristics has been provided in the authors' recently published work [16]. In the same study, the following baseline HTC correlation was derived based on available data for cryogenic fluids:

$$h_{fb} = (0.148 + 0.052\ sin\theta)\ \frac{k_g}{L_b}\left[Ra_g \cdot \left(\frac{h_{fg} + 0.46\ c_{p,g}\left(T_{w,fb} - T_f\right)}{c_{p,g}\left(T_{w,fb} - T_f\right)}\right)\right]^{0.33} + h_r \tag{25}$$

where h_r denotes the radiation HTC, expressed by the following relation:

$$h_r = \frac{(1.7 - 0.55\ sin\theta)\sigma_b\left(T^4_{w,fb} - T^4_f\right)}{\left(T_{w,fb} - T_f\right)} \tag{26}$$

In Eq. (25), h_{fb} represents the overall film boiling (FB) HTC [W.m^{-2}.K^{-1}], accounting for both conduction through the vapor film and thermal radiation effects. The angle θ refers to the orientation angle of the heated surface measured from the horizontal upward position [°], k_g is the thermal conductivity of saturated vapor [W.m^{-1}.K^{-1}], $T_{w,fb}$ is the temperature of the heating surface in the film boiling regime [K], and σ_b is the Stefan–Boltzmann constant, 5.67×10^{-8} W.m^{-2}.K^{-4}. The term L_b, known as the Laplace constant or bubble length [m], is a characteristic length scale that governs vapor film stability and curvature effects, and is calculated using the following relation:

$$L_b = \sqrt{\frac{\sigma}{g(\rho_f - \rho_g)}} \tag{27}$$

Moreover, Ra_g is the Rayleigh number at saturated vapor conditions, which can be determined as:

$$Ra_g = \frac{L_b^3\ \rho_g\ (\rho_f - \rho_g)\ g}{\mu_g^2}\left(\frac{\mu_g\ c_{p,g}}{k_g}\right) \tag{28}$$

Although the above baseline FB correlation achieved an MAE of 12.94 %, it does not account for effects beyond surface orientation and radiation. With the incorporation of recently acquired experimental data and a comprehensive reassessment of the universal database, the FB correlation is further refined to include these additional influencing parameters. This enhancement is aimed at improving predictive accuracy across a broader range of conditions, particularly those relevant to cryogenic thermal system design. The various factors affecting the FB regime will be discussed individually in the following sections, along with the formulation of corresponding multipliers or correction functions to be applied to the baseline correlation.

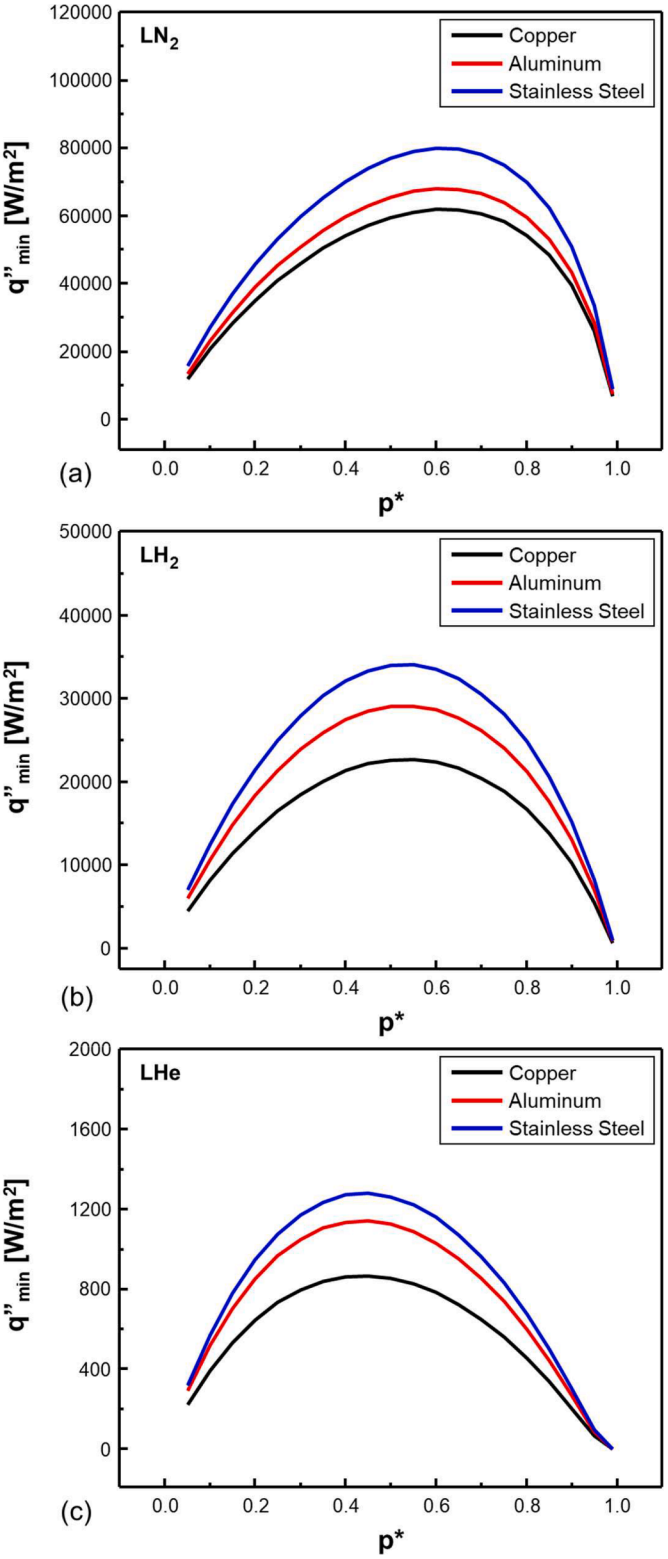

Fig. 13. Variation of q''_{min} with reduced pressure for different surface materials predicted according to newly modified correlation for (a) LN_2, (b) LH_2, and (c) LHe.

2.8.1. Effects of radiation on FB

Although radiation effects were included in the baseline FB correlation, improved formulation was achieved by incorporating additional data points into the universal cryogenic boiling database. As shown in Fig. 14, predictions from the baseline FB correlation were compared to the experimental database for LN_2. It was observed that the correlation tended to underpredict the HTC, particularly at higher wall superheats. This underprediction highlighted a limitation in the original formulation—specifically, the insufficient contribution of the radiation HTC at elevated temperatures where radiative heat transfer becomes increasingly dominant. To address this issue, the radiation term in the correlation was revised. A higher pre-factor was introduced, enhancing the influence of thermal radiation at higher surface temperatures. The updated radiation HTC is now expressed as:

$$h_r = \frac{(3.5 - 0.55\ sin\theta)\sigma_b\left(T_{w,fb}^4 - T_f^4\right)}{\left(T_{w,fb} - T_f\right)} \tag{29}$$

This modification increases the weighting of radiative heat transfer in the overall HTC, particularly for surfaces operating at higher wall superheats. As illustrated in Fig. 14, the updated FB correlation, now incorporating the revised radiation term, exhibits significantly improved agreement with experimental data, especially in the high-temperature regime. This enhancement ensures more accurate predictions across a broader range of operating conditions and more faithfully captures the physical dominance of radiation in the FB regime at elevated wall temperatures.

2.8.2. Effects of heated surface size on FB

In Fig. 15(a), the variation of FB heat flux with wall superheat is compared for three different sizes of heated surfaces, expressed in terms of the dimensionless ratio L_c/λ_d, using LN_2 data from Sauer et al. [43]. It is evident that a substantial enhancement in FB heat transfer occurs as the heated surface size is reduced. This improvement is attributed to the stronger influence of surface edges on smaller heaters, which promote more effective vapor escape and reduce the likelihood of sustained vapor entrapment. Consequently, the insulating vapor layer is partially suppressed, resulting in higher HTCs within the FB regime. Conversely, larger heated surfaces exhibit weaker edge effects, leading to the formation of a thicker and more stable vapor blanket. This vapor layer acts as a significant thermal barrier, impeding liquid–surface contact and thereby reducing the overall heat transfer performance. To quantitatively capture the impact of heater size on film boiling behaviour, a heater-size-based multiplier is proposed, formulated from the expanded FB dataset:

$$F_{S,\ FB} = 1 + 2e^{-0.36\left(\frac{L_c}{\lambda_d}\right)^2} \tag{30}$$

This empirical multiplier adjusts the baseline HTC to account for the enhancement observed in small heaters, which arises from more efficient vapor escape mechanisms at the heated surface edges. These edge-driven effects reduce vapor blanket stability, thereby improving thermal contact between the surface and liquid. The validity and improved predictive capability of this size-based multiplier are demonstrated in Fig. 15(b), where the correlation incorporating the factor $F_{S,FB}$ shows significantly better agreement with experimental data for LH_2 from Kozlov et al. [44], compared to the original correlation without the multiplier.

2.8.3. Effects of surface roughness and material on FB

In the nucleate boiling (NB) regime, bubble formation is strongly influenced by the presence of surface cavities, which act as active nucleation sites and contribute to enhanced HTC. In contrast, the FB regime is characterized by the formation of a continuous vapor blanket that envelops the heated surface, effectively eliminating direct liquid-

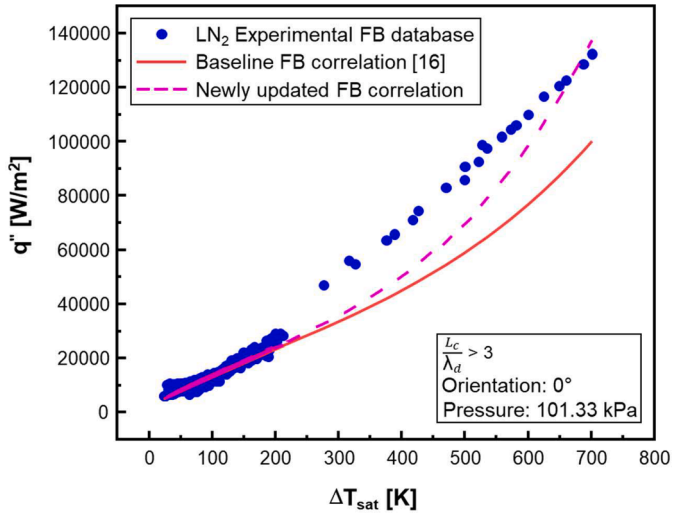

Fig. 14. FB predictions based on baseline and newly updated correlations compared to LN_2. (Data taken from Ahmad et al. [16] consolidated FB database and additional FB data from [43]).

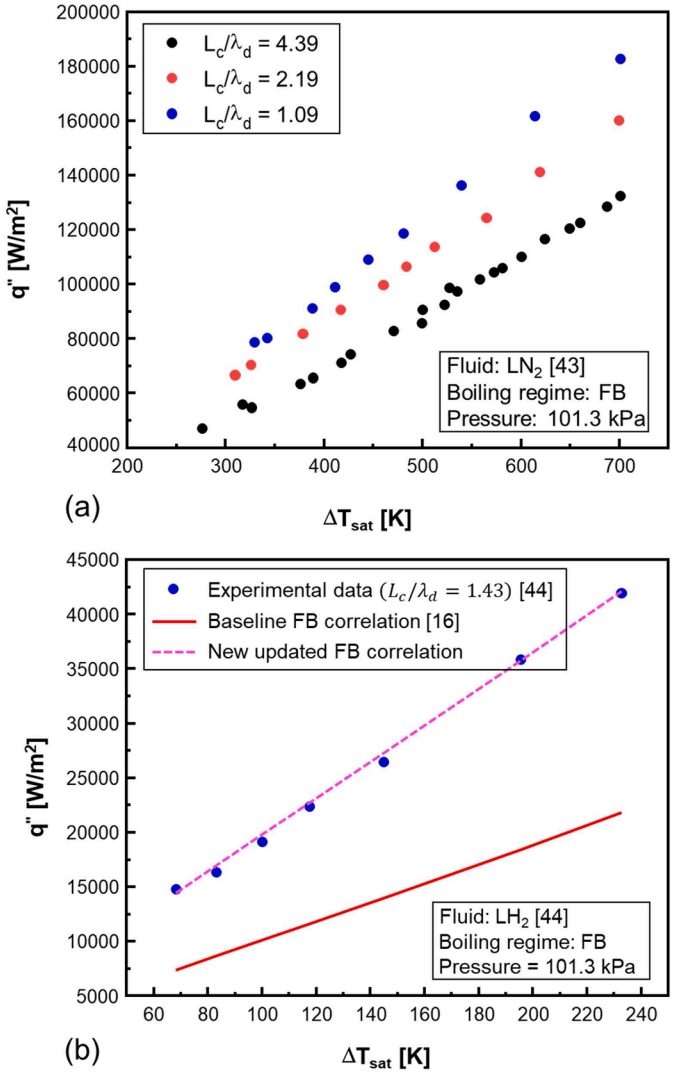

Fig. 15. (a) LN_2 FB data from [43] for different heated surface sizes, (b) FB predictions based on baseline and newly updated correlations compared to LH_2 data from [44].

–surface contact. As a result, microscopic surface features such as roughness exert minimal influence on heat transfer. Due to this diminished effect, and the lack of substantial experimental data in the literature on surface roughness in the FB regime, surface roughness is not incorporated into the updated FB correlation. Moreover, in the lower temperature region of the FB regime, near the MHF point, conduction through the vapor film contributes appreciably to heat transfer. In this region, surfaces composed of materials with higher thermal conductivity promote thinner vapor layers, thereby enhancing heat transfer. However, as the surface temperature rises, radiative heat transfer becomes dominant, and the role of conduction diminishes due to the increasing thickness and stability of the insulating vapor layer. Consequently, the influence of surface material is explicitly accounted for in the updated MHF point correlations, specifically in the formulations for $T_{w,min}$ and q''_{min}. In contrast, it is excluded from the FB correlation, where its impact is negligible at the elevated temperatures that define the upper region of the FB regime.

2.8.4. *Effects of subcooling on FB*

At a given heat flux, the presence of subcooling leads to a lower

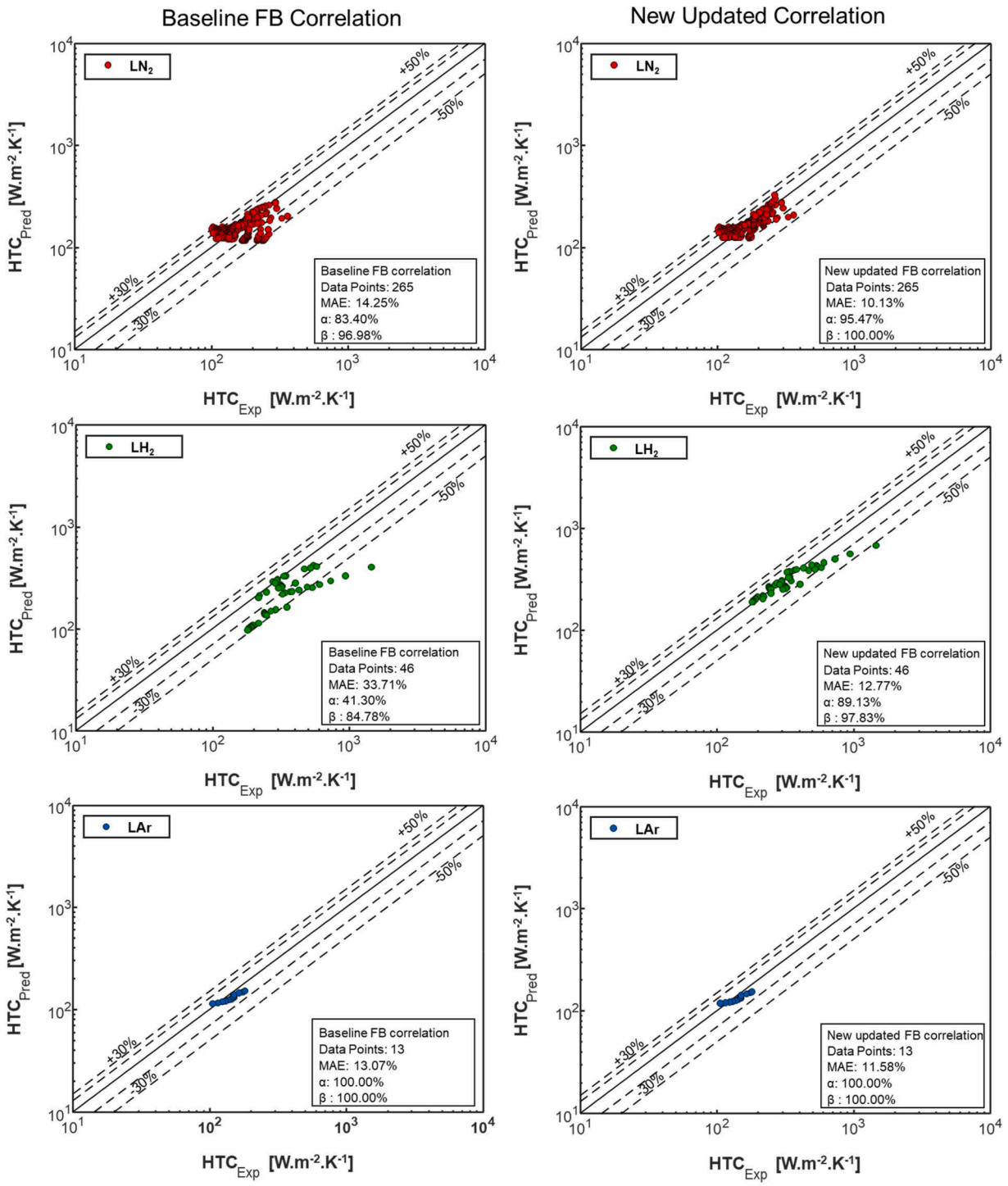

Fig. 16. Comparison of FB HTC predictions across different cryogens using the baseline correlation [16] and new updated correlation. (Data taken from Ahmad et al. [16] FB consolidated database).

Table 2
Summary of new updated correlations for different pool boiling regimes.

Region/Point	Correlation(s)	Application Range	Remarks
Natural convection (NC) region	$h_{nc} = \frac{k_l}{L_c} C\, Ra_L^n$ $Ra_L = \frac{L_c^3\, \rho_L(\rho_L - \rho_{Lw})\, g}{\mu_l^2}\left(\frac{\mu_l\, c_{pl}}{k_l}\right)$	$\Delta T_{sat} \leq \Delta T_{ONB}$	Values for C and n are provided in Table 1.
Onset of nucleate boiling (ONB) point	-	$\Delta T_{sat} = \Delta T_{ONB}$	Intersection point of NC and NB
Nucleate boiling (NB) region	$h_{nb} = 13.3\, q^{''\,0.665}(1 + 0.52\, p^*)^{4.7} Pr_f^{-1.09}\left(1 + 68\, e^{20(p^*-1.1)}\right)$ $\times \left[1 + 1.3\left(\frac{\rho_f}{\rho_g}\right)^{0.4}\left(\frac{c_{p,f}\, \Delta T_{sub}}{h_{fg}}\right)^{3.5}\right]$ $\times \left[1 + \frac{1.5}{1 + e^{-30\,(R_a - 0.32)}}\right]$ $\times \left[\left(\frac{k_w}{k_{Cu}}\right)^m\right]$ $\times [1 + 0.04\, sin\theta]$ Where $m = 0.02$ for smooth surfaces (Ra $\leq$ 0.1 μm) $m = 0.15$ for rough surfaces (Ra $>$ 0.1 μm)	$\Delta T_{ONB} < \Delta T_{sat} < \Delta T_{CHF}$	Effects of subcooling, surface roughness, material, and orientation are included. Effect of heated surface size is not included. Baseline NB HTC correlation is updated by introducing multiplier functions for the above effects.
Critical heat flux (CHF) point	Wall superheat at CHF point $\Delta T_{CHF} = T_{w,CHF} - T_{sat} = \frac{q''_{CHF}}{h_{CHF}}$ Where $h_{CHF} = h_{nb}\big]_{q''_{nb} = q''_{CHF}}$	$\Delta T_{sat} = \Delta T_{CHF}$	$T_{w,CHF}$ is determined by the intersection of the NB curve with the calculated q''_{CHF}.
	Heat flux at CHF point $q''_{CHF} = \left[0.05\left(\frac{p}{p_c}\right)^{0.2} - 0.104\left(\frac{p}{p_c}\right)^{12} + 0.12\right]$ $\times \left[1 - 0.004\left(\frac{p}{p_c}\right)\theta\right]\left\lvert cos\left(\frac{88}{180}\theta\right)\right\rvert^{0.364}$ $\times \left[1 + 0.16\left(\frac{c_{p,f}\, \Delta T_{sub}}{h_{fg}}\right)\right]$ $\times \left[\rho_g h_{fg}\left(\frac{\sigma\, g\, (\rho_f - \rho_g)}{\rho_g^2}\right)^{1/4}\right]\left[\frac{a}{g}\right]^{0.17}$ $\times \left[e^{-1.7\left(\frac{L_c}{3\lambda_d}\right)^{-0.4}} + 1\right]\left[0.49\left(\frac{k_w}{k_f}\right)^{0.065}\right]$		This correlation is taken from the study by Foster et al. [13].
Transition boiling (TB) region	$\Delta T_{tb} = [\Delta T_{CHF} + \varphi\, (\Delta T_{min} - \Delta T_{CHF})]$ $\varphi = \left\lvert\left(\frac{q'' - q''_{CHF}}{q''_{min} - q''_{CHF}}\right)^{0.8}\right\rvert$	$\Delta T_{CHF} \leq \Delta T_{sat} \leq \Delta T_{min}$	Although this correlation itself is not modified, it is indirectly affected due to the updates made to the CHF and MHF correlations.
Minimum heat flux (MHF) point	Wall temperature at MHF point $T_{w,min} = \left[T_{sat} + 1.6\, (T_c - T_{sat})\left(0.15 + 1.74\left(\frac{p}{p_c}\right)^{0.5}\right)\right]\left[\frac{k_{cu}}{1 + k_w}\right]^{0.07}$	$\Delta T_{sat} = \Delta T_{min}$	New correlation is proposed in this study. Effect of heated surface material is included. Subcooling data are not available for T_{min}. Pressure function is incorporated to achieve a MHF trend similar to that of CHF.
	Heat flux at MHF point $q''_{min} = 0.0348\left[\frac{c_{p,\,g}\, k_g^2}{\mu_g}\rho_g\, g(\rho_f - \rho_g)\right]^{0.549}$ $\times \left[0.414\, (\Delta T_{min,\,Cu})^{0.399} - 0.112\right]^{3.1217}$		New correlation is proposed in this study. Effects of subcooling, surface roughness, material, and orientation are included.

(*continued on next page*)

Table 2 (*continued*)

Region/Point	Correlation(s)	Application Range	Remarks
Film boiling (FB) region	$\times \left[1+1.3\left(\frac{\rho_f}{\rho_g}\right)^{0.2}\left(\frac{c_{p,f}\,\Delta T_{sub}}{h_{fg}}\right)\right][1+0.2\sin(1.1\theta)]$ $\times\left[1+2.8\,e^{-0.36\left(\frac{L_c}{\lambda_d}\right)^2}\right]\left[\frac{k_{Cu}}{1+k_w}\right]^{0.07}$ $h_{fb}=\frac{k_g}{L_b}\left[Ra_g\left(\frac{h_{fg}+0.46\,c_{p,g}\,(T_{w,fb}-T_{sat})}{c_{p,g}\,(T_{w,fb}-T_{sat})}\right)\right]^{0.33}$ $\times\left[1+2\,e^{-0.36\left(\frac{L_c}{\lambda_d}\right)^2}\right][0.148+0.052\,\sin\theta]$ $+\left[\frac{(3.5-0.55\,\sin\theta)\,\sigma_b\left(T_{w,fb}^4-T_{sat}^4\right)}{(T_{w,fb}-T_{sat})}\right]$	$\Delta T_{sat} \geq \Delta T_{fb\mid 1.5q''_{min}}$	Effect of heated surface size is incorporated. No subcooled FB data are found so this effect is excluded. Coefficient in radiation term is updated from 1.7 to 3.5. Baseline FB HTC correlation is updated by introducing multiplier functions for the above effects.

required wall superheat compared to saturated conditions. Under such conditions, the cooler liquid in contact with the vapor layer facilitates partial condensation of the vapor, resulting in a thinner and less stable vapor film. This disruption of the vapor blanket enhances liquid–surface interaction, thereby improving overall heat transfer performance in the FB regime. However, to quantitatively evaluate the extent of this enhancement, experimental data specific to subcooled film boiling are essential. A comprehensive literature survey conducted as part of this study did not identify any such data across cryogenic or conventional fluids. Consequently, no subcooling multiplier is proposed in the present work for the film boiling regime. This gap highlights an important opportunity for future research. Targeted experimental investigations under subcooled conditions are needed to assess the impact on film stability and heat transfer, and to formulate an appropriate empirical multiplier that can be incorporated into generalized FB correlations.

2.8.5. Final updated film boiling HTC correlation

The aforementioned effects of radiation and heated surface size are systematically incorporated in the development of the following updated FB correlation:

$$h_{fb}=\frac{k_g}{L_b}\left[Ra_g\cdot\left(\frac{h_{fg}+0.46\,c_{p,g}\,(T_{w,fb}-T_{sat})}{c_{p,g}\,(T_{w,fb}-T_{sat})}\right)\right]^{0.33}$$
$$\times\left[1+2e^{-0.36\left(\frac{L_c}{\lambda_d}\right)^2}\right][0.148+0.052\,\sin\theta] \quad (31)$$
$$+\left[\frac{(3.5-0.55\,\sin\theta)\sigma_b\left(T_{w,fb}^4-T_{sat}^4\right)}{(T_{w,fb}-T_{sat})}\right]$$

In this expression, the heater size multiplier from Eq. (30) is incorporated to capture surface size effects, while the revised radiation term from Eq. (29) accounts for the enhanced radiative contribution at elevated wall superheats, as previously discussed. The performance of this updated FB correlation is evaluated using an expanded experimental database encompassing a broad range of operating conditions and cryogenic fluids. As illustrated in Fig. 16, predictions from both the baseline correlation [16] and the newly updated FB formulation are compared against experimental data for LN_2, LH_2, and LAr. The updated correlation demonstrates a clear quantitative improvement in predictive accuracy across all cryogens considered. For LN_2, the MAE is reduced from 14.25 % to 10.13 %, while for LH_2 the MAE decreases substantially, from 33.71 % to 12.77 %. A modest improvement is also observed for LAr, with the MAE reduced from 13.07 % to 11.58 %. These reductions in error confirm the enhanced agreement between predictions and experimental data achieved by the updated correlation, particularly for LH_2 and LN_2, thereby strengthening its suitability for practical cryogenic thermal applications.

The summary of all the updated correlations along with thier application range are presented in Table 2.

3. Summary of strengths, limitations, and future recommendations

3.1. Strengths of the present methodology

The strengths of this study have been thoroughly discussed in the preceding sections. However, the key merits that distinguish the present work from existing literature are highlighted and summarized below:

- A key strength of the proposed methodology lies in its integration of data from a wide array of cryogenic experiments. This approach bypasses the significant time and cost associated with conducting a single, large-scale experiment that accounts for all influencing

factors. By systematically combining and analyzing results from diverse experimental sources, the study reveals broader trends and insights that would be difficult to extract from isolated datasets. This data-driven strategy enhances the generality, efficiency, and practical relevance of the proposed correlations and predictive framework.

- Unlike previous experimental studies that typically examine the effect of a single parameter while holding others constant, the present work systematically investigates the influence of multiple critical parameters (including pressure, subcooling, heated surface material, surface roughness, size, and orientation) on different regimes of pool boiling. This comprehensive approach enables a more complete and nuanced understanding of boiling behaviour across a broad range of operating conditions.

3.2. Limitations of the present study

While the present study offers a comprehensive framework to analyze all regimes of the pool boiling curve across various influencing parameters, certain limitations must be acknowledged to provide a balanced perspective:

- As the present methodology integrates data from multiple independent experiments, exact one-to-one (apple-to-apple) comparisons are not always feasible. For example, when evaluating the effect of surface roughness, other parameters—such as material type, surface size, or orientation—may vary across the referenced datasets. As a result, it may not always be possible to isolate and conclusively attribute observed trends to a single parameter.
- Although updated correlations for all boiling regimes were developed in this study, the underlying datasets were drawn from independent experimental studies available in the literature. These datasets were obtained from experiments conducted in different laboratories, each employing its own equipment, measurement techniques, and experimental protocols. Consequently, even when the reported operating and geometric conditions appear identical, slight differences in surface preparation, ambient conditions, instrumentation, or calibration procedures can introduce noticeable variations in the measured boiling behaviour.
- For several cryogenic fluids, particularly at higher reduced pressures, experimental data are limited or entirely unavailable. As a result, the derived correlations may exhibit reduced accuracy in these underexplored regions and should be applied with appropriate caution in such cases. These regions are already explained in the author's previous papers with the help of parametric distribution of databases [11–16].
- The multipliers used to account for various parameter effects were developed based on limited experimental data. In certain cases, such as the FB regime and the wall temperature at the MHF point (T_{min}), reliable experimental data capturing the influence of subcooling are currently unavailable in the literature. Consequently, these effects were not incorporated into the present study. Future refinements are recommended as additional high-quality data become available.

3.3. Future recommendations

Based on the limitations and key findings of the present study, the following areas are identified as priorities for future research to further improve the accuracy, applicability, and robustness of the proposed correlations:

1. Future experimental efforts should prioritize generating complete boiling curves under well-defined operating conditions, rather than limiting investigations to individual regimes (e.g., NB, TB, or FB) or specific transition points (e.g., ONB, CHF, or MHF). Comprehensive datasets of this nature will ensure greater consistency and enable more accurate development and validation of boiling correlations across all regimes.
2. For most cryogenic fluids (excluding LHe) available experimental data are largely confined to low pressures. Future research should focus on developing experimental setups capable of operating at elevated pressures, particularly near the critical point. Such efforts are essential for improving the understanding and prediction of cryogenic boiling behaviour in high-pressure regimes, where current correlations are limited by data scarcity.
3. Critical data gaps remain in the literature, particularly regarding the effect of subcooling on the FB regime and the MHF point. Targeted experimental studies are needed to generate high-quality data in these underexplored areas, which are essential for improving the completeness and accuracy of boiling correlations across all regimes.
4. As more experimental data become available, the present correlations, particularly the multipliers used to capture the effects of various parameters, should be revisited and refined. To further enhance model accuracy and predictive capability, future efforts could incorporate machine learning or other artificial intelligence-based techniques to identify complex, non-linear relationships within the expanded datasets.
5. All correlations developed in this study, except for q''_{CHF}, are formulated based on terrestrial gravity conditions. To extend their applicability to space-based systems, gravity scaling must be performed. This requires incorporating experimental data from microgravity pool boiling studies to appropriately adjust the correlations for reduced-gravity environments.

4. Conclusions

This study represents a significant advancement in the ongoing collaborative effort, initiated in 2018, between the Purdue University Boiling and Two-Phase Flow Laboratory (PU-BTPFL) and NASA Glenn Research Center. The overarching goal of this initiative has been to develop predictive correlations for all regimes and transition points of the pool boiling curve for cryogenic fluids. While earlier studies [11–16] successfully established baseline correlations under saturated conditions, and a methodology was proposed in [17] to construct the complete boiling curve, the effects of key practical parameters—such as subcooling, surface roughness, heated surface material, size, and orientation—had not yet been systematically incorporated. The present study fills this important gap by drawing on a wide range of experimental data from the literature to quantify the influence of these parameters and integrate them into the existing framework. Key conclusions from this study are summarized below:

1. The minimum dimension of the heated surface (L_c) has a significant impact on the heat flux at the CHF and MHF points, as well as the HTC in the FB regime. These quantities were observed to decrease as the ratio L_c/λ_d increases, exhibiting asymptotic behaviour that becomes negligible when L_c exceeds approximately $3\lambda_d$. Due to inconsistent trends in the NB regime, this effect was not incorporated into the NB correlation. In the NC regime, the influence of L_c was found to be non-monotonic and dependent on surface orientation and operating conditions.
2. Subcooling was found to enhance the HTC across all boiling regimes by reducing the required wall superheat at a given heat flux. A subcooling multiplier was developed to capture this trend and was successfully incorporated into the correlations for the NB regime and CHF. However, due to the lack of reliable experimental data, subcooling effects were not incorporated into the FB regime or the wall temperature at the MHF point (T_{min}). These areas remain open for future experimental validation and correlation refinement.
3. Surface roughness has a dominant influence on the NB regime by increasing the number of active nucleation sites. This effect was incorporated into the NB HTC correlation through a roughness

multiplier. In contrast, no significant effect was assumed for the FB regime due to the absence of direct liquid–surface contact. The influence of surface roughness on the CHF remains inconclusive, as the available data exhibit conflicting trends; consequently, this effect was omitted from the current investigation.

4. The thermal conductivity of the heated surface plays a significant role across most boiling regimes by promoting more uniform heat distribution, thereby enhancing boiling performance. The exception is the FB regime, which remains unaffected due to the lack of direct contact between the heated surface and the liquid.
5. Surface orientation was found to influence all boiling regimes and transition points. However, its effect is relatively minor in the NB regime compared to its more pronounced impact on the NC and FB regimes and CHF.

Author declaration

We wish to confirm that there are no known conflicts of interest associated with this publication and there has been no significant financial support for this work that could have influenced its outcome.

We confirm that the manuscript has been read and approved by all named authors and that there are no other persons who satisfied the criteria for authorship but are not listed. We further confirm that the order of authors listed in the manuscript has been approved by all of us.

We confirm that we have given due consideration to the protection of intellectual property associated with this work and that there are no impediments to publication, including the timing of publication, with respect to intellectual property. In so doing we confirm that we have followed the regulations of our institutions concerning intellectual property.

We understand that the Corresponding Author is the sole contact for the Editorial process (including Editorial Manager and direct communications with the office). He is responsible for communicating with the other authors about progress, submissions of revisions and final approval of proofs. We confirm that we have provided a current, correct email address which is accessible by the Corresponding Author and which has been configured to accept email from mudawar@ecn.purdue.edu

CRediT authorship contribution statement

Faraz Ahmad: Writing – review & editing, Writing – original draft, Validation, Software, Methodology, Investigation, Formal analysis, Data curation, Conceptualization. **Issam Mudawar:** Writing – review & editing, Writing – original draft, Validation, Supervision, Resources, Project administration, Methodology, Investigation, Funding acquisition, Formal analysis, Conceptualization. **Michael Meyer:** Writing – review & editing, Writing – original draft, Validation, Supervision, Resources, Project administration, Investigation, Funding acquisition, Formal analysis, Conceptualization. **Jason Hartwig:** Writing – review & editing, Writing – original draft, Validation, Supervision, Resources, Project administration, Methodology, Investigation, Funding acquisition, Formal analysis, Conceptualization.

Declaration of competing interest

The authors declare the following financial interests/personal relationships which may be considered as potential competing interests:

Issam Mudawar reports financial support was provided by NASA Glenn Research Center. Jason Hartwig reports a relationship with NASA Glenn Research Center that includes: employment. If there are other authors, they declare that they have no known competing financial interests or personal relationships that could have appeared to influence the work reported in this paper.

Acknowledgments

The authors are grateful for financial support of the National Aeronautics and Space Administration (NASA) Small Business Technology Transfer (STTR) program under a subcontract from MTS Inc. Phase II contract 80NSSC23CA009. We also thank the Fulbright Program for providing a scholarship for the first author.

References

[1] T.J. LaClair, I. Mudawar, Thermal transients in a capillary evaporator prior to the initiation of boiling, Int. J. Heat. Mass Transf. 43 (2000) 3937–3952.
[2] G. Liang, I. Mudawar, Pool boiling critical heat flux (CHF) – part 2: assessment of models and correlations, Int. J. Heat. Mass Transf. 117 (2018) 1368–1383.
[3] I. Mudawar, R.A. Houpt, Mass and momentum transport in smooth falling liquid films laminarized at relatively high reynolds numbers, Int. J. Heat. Mass Transf. 36 (1993) 3437–3448.
[4] T.C. Willingham, I. Mudawar, Channel height effects on forced-convection boiling and critical heat flux from a linear array of discrete heat sources, Int. J. Heat. Mass Transf. 35 (1992) 1865–1880.
[5] C.O. Gersey, I. Mudawar, Effects of heater length and orientation on the trigger mechanism for near-saturated flow boiling critical heat flux - II. Critical heat flux model, Int. J. Heat. Mass Transf. 38 (1995) 643–654.
[6] S. Mukherjee, I. Mudawar, Pumpless loop for narrow channel and micro-channel boiling from vertical surfaces, J. Electron. Packag. 125 (2003) 431–441.
[7] M.T. Meyer, I. Mudawar, C.E. Boyack, C.A. Hale, Single and two-phase cooling with an array of rectangular jets, Int. J. Heat. Mass Transf. 49 (2006) 17–29.
[8] I. Mudawar, T.A. Deiters, A universal approach to predicting temperature response of metallic parts to spray quenching, Int. J. Heat. Mass Transf. 37 (1994) 347–362.
[9] S. Kim, F. Ahmad, I. Mudawar, J. Hartwig, Computational investigation of the effects of gravity on cryogenic flow boiling, Appl. Therm. Eng. (2025) 128663.
[10] E.W. Lemmon, I.H. Bell, M.L. Huber, M.O. McLinden, NIST Standard Reference Database 23: Reference Fluid Thermodynamic and Transport properties-REFPROP, Version 10.0, National Institute of Standards and Technology, Gaithersburg, 2018. Standard Reference Data Program.
[11] F. Ahmad, S. Kim, M. Meyer, J. Hartwig, I. Mudawar, Saturated nucleate pool boiling of cryogenic fluids: review of databases, assessment of existing models and correlations, and development of new universal correlation, Int. J. Heat. Mass Transf. 231 (2024) 125807.
[12] R. Patel, M. Meyer, J. Hartwig, I. Mudawar, Review of cryogenic pool boiling critical heat flux databases, assessment of models and correlations, and development of new universal correlations, Int. J. Heat. Mass Transf. 190 (2022) 122579.
[13] D. Foster, S. Darges, N. Damle, S. Kim, I. Mudawar, J. Hartwig, Experimental investigation of LN_2 pool boiling critical heat flux (CHF) and development of new correlation for all cryogens, accounting for effects of surface material and size, pressure, subcooling, and surface orientation, Int. J. Heat. Mass Transf. 254 (2026) 127590.
[14] F. Ahmad, M. Meyer, J. Hartwig, I. Mudawar, Development of new correlations for critical heat flux point wall temperature and transition boiling under steady-state saturated pool boiling of cryogens, Int. J. Heat. Mass Transf. 239 (2025) 126592.
[15] F. Ahmad, M. Meyer, J. Hartwig, I. Mudawar, Development of new universal correlations for minimum heat flux point for saturated pool boiling of cryogens, Int. J. Heat. Mass Transf. 234 (2024) 126099.
[16] F. Ahmad, M. Meyer, J. Hartwig, I. Mudawar, Saturated pool film boiling of cryogenic fluids: review of databases, assessment of existing models and correlations, and development of new universal correlation, Int. J. Heat. Mass Transf. 235 (2024) 126190.
[17] F. Ahmad, D. Foster, S. Kim, M. Meyer, J. Hartwig, I. Mudawar, Method for generating a complete saturated pool boiling curve for cryogenic fluids under terrestrial gravity, Int. J. Heat. Mass Transf. 243 (2025) 126876.
[18] I.L. Pioro, W. Rohsenow, S.S. Doerffer, Nucleate pool-boiling heat transfer. I: review of parametric effects of boiling surface, Int. J. Heat. Mass Transf. 47 (2004) 5033–5044.
[19] L. Wang, Y. Li, F. Zhang, F. Xie, Y. Ma, Correlations for calculating heat transfer of hydrogen pool boiling, Int. J. Hydrog. Energy 41 (2016) 17118–17131.
[20] F.P. Incropera, D.P. DeWitt, T.L. Bergman, A.S. Lavine, Fundamentals of Heat and Mass Transfer, Wiley, New York, 1996.
[21] J.R. Lloyd, W.R. Moran, Natural convection adjacent to horizontal surface of various planforms, J. Heat. Trans. 96 (1974) 443–447.
[22] W.H. McAdams, Heat Transmission, McGraw-Hill, 1954.
[23] F.J. Bayley, An analysis of turbulent free-convection heat-transfer, Proc. Inst. Mech. Eng. 169 (1955) 361–370.
[24] E. Radziemska, W.M. Lewandowski, Heat transfer by natural convection from an isothermal downward-facing round plate in unlimited space, Appl. Energy 68 (2001) 347–366.
[25] E.S. Gadelmawla, M.M. Koura, T.M.A. Maksoud, I.M. Elewa, H.H. Soliman, Roughness parameters, J. Mater. Proc. Tech. 123 (2002) 133–145.
[26] C. Cai, I. Mudawar, H. Liu, C. Si, Theoretical Leidenfrost point (LFP) model for sessile droplet, Int. J. Heat. Mass Transf. 146 (2020) 118802.
[27] S. Nishio, G.R. Chandratilleke, Steady-state pool boiling heat transfer to saturated liquid helium at atmospheric pressure, JSME Int. J 32 (1989) 639–645.

[28] V.A. Grigoriev, Y.M. Pavlov, E.V. Ametistov, An investigation of nucleate boiling heat transfer of helium, int, in: Heat Transfer Conf. Digital Library, Begel House, 1974.
[29] I.P. Vishnev, V.V. Corokhov, G.G. Svalov, Study of heat transfer in boiling of helium on surfaces with various orientations, Heat Transf. – Sov. Res 8 (1976) 104–108.
[30] E.A. Ibrahim, R.W. Boom, G.E. McIntosh, Heat transfer to subcooled liquid helium, Adv. Cryog. Eng 23 (1978) 333–339.
[31] Y. Shirai, H. Tatsumoto, M. Shiotsu, K. Hata, H. Kobayashi, Y. Naruo, Y. Inatani, Boiling heat transfer from a horizontal flat plate in a pool of liquid hydrogen, Cryog. (Guildf) 50 (2010) 410–416.
[32] K. Ferjančič, I. Golobič, Surface effects on pool boiling CHF, Exp. Therm. Fluid. Sci. 25 (2002) 565–571.
[33] T.G. Theofanous, T.-N. Dinh, J.P. Tu, A.T. Dinh, The boiling crisis phenomenon: part II: dryout dynamics and burnout, Exp. Therm. Fluid. Sci. 26 (2002) 793–810.
[34] X. Fan, S. Gu, J. Lei, G. Luo, F. Meng, L. Wu, S. Gu, Experimental and analytical study on the influence of saturation pressure and surface roughness on pool boiling CHF of HFE-7100, Int J Chem Eng (2022) 4875208.
[35] H. O'Hanley, C. Coyle, J. Buongiorno, T. McKrell, L.W. Hu, M. Rubner, R. Cohen, Separate effects of surface roughness, wettability, and porosity on the boiling critical heat flux, Appl. Phys. Lett. 103 (2013).
[36] P.J. Berenson, Experiments on pool-boiling heat transfer, Int. J. Heat. Mass Transf. 5 (1962) 985–999.
[37] P.F. Alvariño, M.L.S. Simón, M. dos Santos Guzella, J.M.A. Paz, J.M.S. Jabardo, L. C. Gómez, Experimental investigation of the CHF of HFE-7100 under pool boiling conditions on differently roughened surfaces, Int. J. Heat. Mass Transf. 139 (2019) 269–279.
[38] J.H. Lienhard, V.K. Dhir, D.M. Riherd, Peak pool boiling heat-flux measurements on finite horizontal flat plates, J. Heat. Transf. 95 (1973) 477–482.
[39] V.G. Morozov, An experimental investigation of the cessation of film boiling of a liquid on a submerged heating surface, Int. Chem. Eng 3 (1963) 48–51.
[40] S.S. Kutateladze, On the transition to film boiling under natural convection, Kotloturbostroenie 3 (1948) 10.
[41] N. Zuber, Hydrodynamic aspects of boiling heat transfer, Univ. of California, Los Angeles, US Atomic Energy Commission, Technical Information Service, 1959. Report No. AECU-4439.
[42] I. Mudawar, A.H. Howard, C.O. Gersey, An analytical model for near-saturated pool boiling critical heat flux on vertical surfaces, Int. J. Heat. Mass Transf. 40 (1997) 2327–2339.
[43] H.J. Sauer Jr, K.M. Ragsdell, Film pool boiling of nitrogen from flat surfaces, in: Proc. 1970 Cryogenic Eng. Conf., Boulder, Colorado, June 17–17, 1970, pp. 412–415.
[44] S.M. Kozlov, S.V. Nozdrin, Heat transfer and boundaries of its regimes during hydrogen boiling at different metallic surfaces, Cryog. (Guildf) 32 (1992) 245–248.